Imaging endogenous synaptic proteins in primary neurons at single-cell resolution using CRISPR/Cas9

Takahiko Matsuda[a] and Izumi Oinuma[a,b,*]
[a]Laboratory of Cell and Molecular Biology, Graduate School of Life Science, University of Hyogo, Hyogo 678-1297, Japan; [b]Institute for Integrated Cell-Material Sciences (iCeMS), Kyoto University, Kyoto 606-8501, Japan

ABSTRACT **Fluorescence imaging at single-cell resolution is a crucial approach to analyzing the spatiotemporal regulation of proteins within individual cells of complex neural networks. Here we present a nonviral strategy that enables the tagging of endogenous loci by CRISPR/Cas9-mediated genome editing combined with a nucleofection technique. The method allowed expression of fluorescently tagged proteins at endogenous levels, and we successfully achieved tagging of a presynaptic protein, synaptophysin (Syp), and a postsynaptic protein, PSD-95, in cultured postmitotic neurons. Superresolution fluorescence microscopy of fixed neurons confirmed the identical localization patterns of the tagged proteins to those of endogenous ones verified by immunohistochemistry. The system is also applicable for multiplexed labeling and live-cell imaging. Live imaging with total internal reflection fluorescence microscopy of a single dendritic process of a neuron double-labeled with Syp-mCherry and PSD-95-EGFP revealed the previously undescribed dynamic localization of the proteins synchronously moving along dendritic shafts. Our convenient and versatile strategy is potent for analysis of proteins whose ectopic expressions perturb cellular functions.**

Monitoring Editor
Paul Forscher
Yale University

Received: Apr 22, 2019
Revised: Jul 24, 2019
Accepted: Sep 3, 2019

INTRODUCTION

Fluorescence live-cell imaging at a single-cell resolution with high contrast and specificity is a challenging but indispensable approach to analyze the spatiotemporal regulation of protein localization and function within individual cells of complex neural networks. Several viral and nonviral fluorescent labeling methods are available; however, current methods have significant problems when we intend to perform live-cell imaging of proteins of interest within individual cells forming complex neural networks. Currently available and commonly used labeling methods include immunostaining of endogenous proteins with antibodies specific to target proteins and ectopic expression of fluorescently tagged proteins. Antibody staining usually requires fixation and permeabilization of cells and therefore generally incompatible with live-cell imaging except for the cases where targets are cell surface proteins. Moreover, with antibodies, it is hard to label individual cells sparsely and randomly to visualize cell morphology. Sparse transfection methods have been developed for single-cell labeling, however, ectopic expression of fluorescently tagged target proteins by transfecting exogenous genes often causes overexpression and mistargeting of the proteins, and it is hard to reproduce the expression levels and patterns of target proteins faithfully. Overexpressed or aberrantly localized exogenous proteins sometimes cause undesirable side effects. For example, in the case of PSD-95, a major scaffold protein in the excitatory postsynaptic density (PSD), overexpression of fluorescent protein-tagged PSD-95 in neurons increases the number and size of dendritic spines, alters synaptic currents, and impairs synaptic plasticity (El-Husseini *et al.*, 2000; Béïque and Andrade, 2003; Stein *et al.*, 2003; Ehrlich and Malinow, 2004; Fortin *et al.*, 2014). For

This article was published online ahead of print in MBoC in Press (http://www.molbiolcell.org/cgi/doi/10.1091/mbc.E19-04-0223) on September 11, 2019.
The authors declare no competing financial interests.
Author contributions: T. M. and I. O. designed the research, performed the experiments, analyzed the data, and wrote the manuscript.
*Address correspondence to: Izumi Oinuma (izumi@sci.u-hyogo.ac.jp).
Abbreviations used: ANOVA, analysis of variance; BDNF, brain-derived neurotrophic factor; CRISPR, clustered regularly interspaced short palindromic repeats; DIV, days in vitro; EMCCD, electron-multiplying charge-coupled device; F-actin, filamentous-actin; FBS, fetal bovine serum; gRNA, guide RNA; HDR, homology-directed repair; indel, insertion/deletion; NHEJ, nonhomologous end-joining; PBS, phosphate-buffered saline; PFA, paraformaldehyde; PLL, poly-L-lysine; PSD, postsynaptic density; RT-PCR, reverse transcription-PCR; Syp, synaptophysin; TBS, Tris-buffered saline; TIRF, total internal reflection fluorescence.

this reason, PSD-95 is known as a "problematic protein" to analyze the dynamic localization under physiological conditions in neurons. To overcome the problems, several methods have been recently developed for single-cell labeling of endogenous synaptic proteins by using recombinant antibody-like probes or generating conditional knock-in mice sparsely expressing fluorescently tagged proteins (Gross *et al.*, 2013; Fortin *et al.*, 2014). However, these techniques are usually costly and time-consuming and lack convenience and versatility. None of the present methods provides high-throughput tools for examination of various endogenous proteins in cultured postmitotic neurons.

To genetically label gene products rapidly and specifically, the genome editing technologies using the engineered programmable nucleases have been developed and applied to a variety of cell lines and animals (Gaj *et al.*, 2013). The use of the clustered regularly interspaced short palindromic repeats (CRISPR)-associated endonuclease system (Jinek *et al.*, 2012; Cong *et al.*, 2013; Mali *et al.*, 2013) is becoming widespread; however, current studies have been predominantly focused on dividing cells. CRISPR/Cas9 induces targeted DNA double-strand breaks in the genome, which can be cell-autonomously repaired by nonhomologous end-joining (NHEJ) or homology-directed repair (HDR) (Cong *et al.*, 2013; Mali *et al.*, 2013; Yang *et al.*, 2013; Doudna and Charpentier, 2014; Hsu *et al.*, 2014; Sander and Joung, 2014; Cox *et al.*, 2015). NHEJ can occur throughout the cell cycle, whereas HDR is believed to be absent during the G1 phase of the cell cycle (Heyer *et al.*, 2010; Iyama and Wilson 3rd, 2013). This suggests that homologous recombination is not operational in postmitotic neuronal cells due to the inefficient recruitment of the HDR repair machinery in target cells (Saleh-Gohari and Helleday, 2004; Hsu *et al.*, 2014; Chu *et al.*, 2015; Cox *et al.*, 2015; Maruyama *et al.*, 2015; Heidenreich and Zhang, 2016). The CRISPR/Cas9-mediated genome-editing technology has been useful to introduce NHEJ-mediated insertion/deletion (indel) mutations into genomes in neurons in vitro and in vivo (Incontro *et al.*, 2014; Straub *et al.*, 2014; Wang *et al.*, 2014; Swiech *et al.*, 2015; Shinmyo *et al.*, 2016). Targeted insertion of a sequence through HDR had been supposed to be impossible in the mammalian brain in vivo (Platt *et al.*, 2014; Xue *et al.*, 2014; Yin *et al.*, 2014; Heidenreich and Zhang, 2016), before endogenous protein tagging methods in various brain regions by CRISPR/Cas9-mediated HDR with synthetic single-stranded donor DNA oligo and plasmid-based donor were reported recently (Mikuni *et al.*, 2016; Tsunekawa *et al.*, 2016; Uemura *et al.*, 2016). These methods work sufficiently for sparse fluorescent labeling in the brain in vivo; however, a method for tagging endogenous proteins in primary cultured postmitotic neurons at a single-cell level in vitro has not yet been developed.

Here, we demonstrate the HDR-mediated fluorescent tagging of endogenous synaptic proteins in cultured postmitotic neurons with a combined method of the CRISPR/Cas9 genome-editing technology and the highly efficient nucleofection technique. We achieved the labeling of the proteins at the single-cell level without perturbing the density and size of dendritic spines. The labeling method is compatible with high-resolution imaging of fixed-cells with super-resolution fluorescence microscopy and imaging of live-cell dynamics with total internal reflection fluorescence (TIRF) microscopy. It could also follow transcriptional and translational expression changes in response to synaptic stimuli and brain-derived neurotrophic factor (BDNF). Our method would provide a high-throughput approach for examination of various endogenous proteins, including "difficult proteins" whose ectopic expression perturbs cellular functions.

RESULTS

Fluorescent labeling of endogenous synaptic proteins in primary rat neurons

To perform fluorescent tag knock-in in primary cultured neurons, we utilized a combined method of the CRISPR/Cas9 genome-editing technology and nucleofection, an improved electroporation technique. Most transfection procedures deliver plasmid DNA preferentially into the cytoplasm, and the DNA can enter the nucleus only during cell division when the nuclear envelope is disintegrated, whereas the nucleofection technology enables the DNA to enter directly into the nucleus through the nuclear membrane independently of cell proliferation (Distler *et al.*, 2005). We dissected the cortex and hippocampus from embryonic day 18 (E18) rat brain, and enzymatically dissociated neurons were transfected by nucleofection and cultured for about 3 wk to follow the maturation (Figure 1A).

A postsynaptic protein, PSD-95, and a presynaptic protein, synaptophysin (Syp), were chosen as targets, and the CRISPR guide RNAs (gRNAs) were designed to target the genome sequences of the exons containing the stop codons of the *PSD-95* and *Syp* genes. We prepared two gRNAs for each gene and used together to achieve higher editing efficiency (Figure 1, B and C; for details, see Figure 2, A and F). The targeting vectors were designed to express C-terminal fluorescent fusion proteins of PSD-95-mCherry and Syp-EGFP from the endogenous loci on integration into the genome (Figure 1, B and C). By Western blot analysis of whole-cell lysates prepared from 3-wk-old primary cultures of rat cortical and hippocampal neurons, we detected the production of fluorescent fusion proteins of PSD-95-mCherry and Syp-EGFP in a CRISPR/Cas9-dependent manner (Figure 1, D and E). By immunostaining performed on the fixed primary cultures using anti-mCherry and anti-EGFP antibodies, we detected fluorescence signals in a sparse subset of neurons only in the presence of the CRISPR constructs. We also observed that expression patterns of PSD-95-mCherry and Syp-EGFP in neurons were identical to those of endogenous ones immunostained with antibodies specific to PSD-95 and Syp, respectively, and that these fluorescent fusion proteins showed postsynaptic spine-like punctate staining and presynaptic bouton-like staining, respectively (Figure 1, F and G; Supplemental Figure S1).

Validation of CRISPR/Cas9-mediated fluorescent gene knock-in in cultured neurons

To confirm the correct integration of the targeting vectors into the *PSD-95* and *Syp* loci, we performed genomic analysis of cultured cells. We designed the PCR primer sets to detect the mCherry knock-in allele of *PSD-95* and the EGFP knock-in allele of *Syp* (Figure 2, A and F) and performed PCR using genomic DNA samples isolated from the cultured neurons at 21 d in vitro (DIV) as templates. In parallel, we performed PCR with the primers to detect the targeting vectors, for monitoring plasmid transfection efficiency, and with the primers to detect endogenous rat *Actb* for loading control. With the primers to detect the knock-in alleles, the DNA fragments of the expected size (1285 base pairs) were amplified from the cortical and hippocampal neuron cultures transfected with PSD-95 targeting vector (mCherry) and CBh-Cas9 with gRNAs for *PSD-95* (Figure 2, D and E), and the DNA fragments of the expected size (1367 base pairs) were amplified from the cortical and hippocampal neuron cultures transfected with Syp targeting vector (EGFP) and CBh-Cas9 with gRNAs for *Syp* (Figure 2G, H), suggesting the correct gene knock-in.

We also tested whether endogenous PSD-95 and Syp can be tagged with different fluorescent proteins. For this purpose, PSD-95 targeting vector (EGFP) and Syp targeting vector (mCherry) were

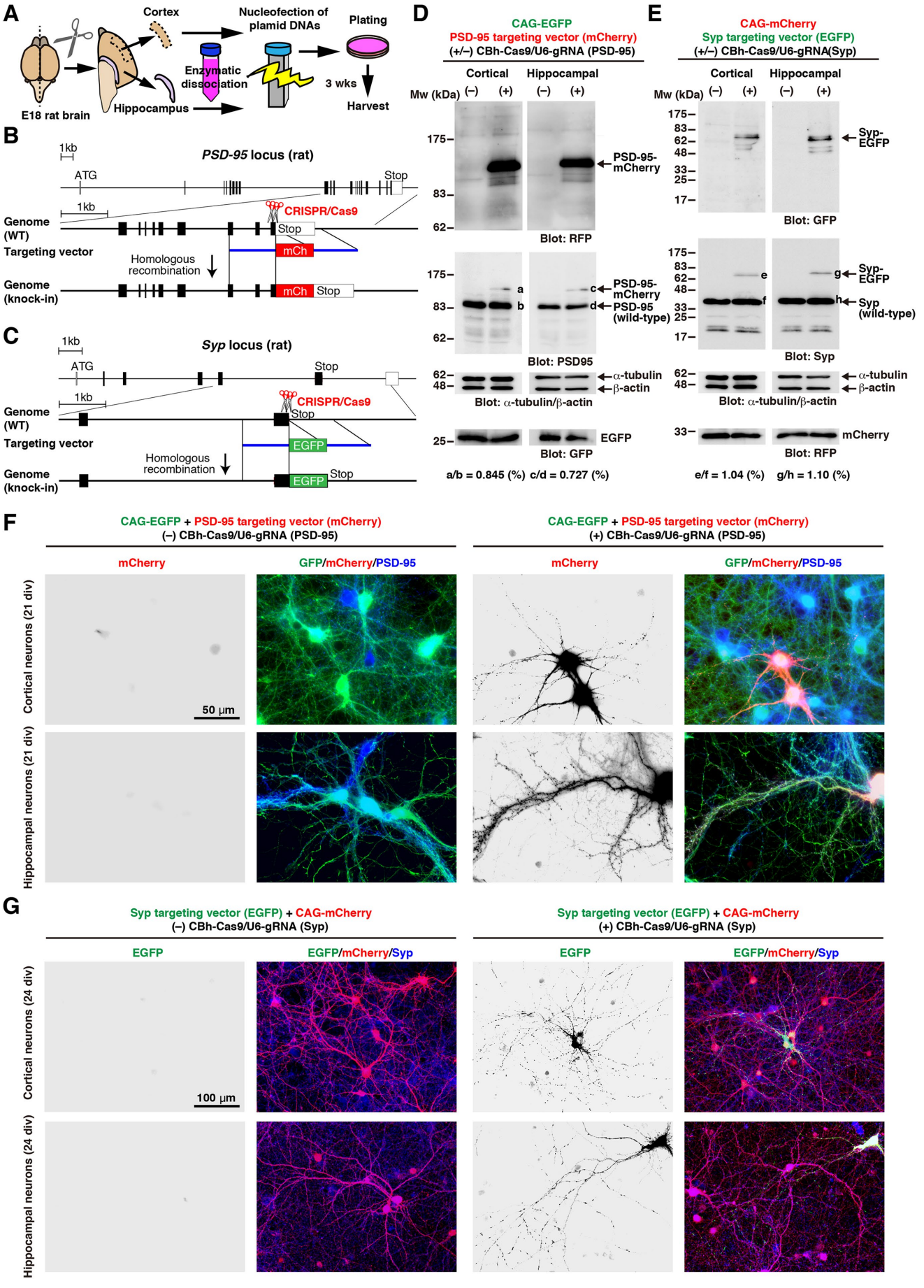
A
Cortex
Nucleofection of plamid DNAs
Plating
Enzymatic dissociation
3 wks
E18 rat brain
Hippocampus
Harvest
B
PSD-95 locus (rat)
1kb
ATG
Stop
CRISPR/Cas9
Genome (WT)
Targeting vector
mCh
Homologous recombination
Genome (knock-in)
C
Syp locus (rat)
EGFP
D
CAG-EGFP
PSD-95 targeting vector (mCherry)
(+/–) CBh-Cas9/U6-gRNA (PSD-95)
Cortical
Hippocampal
Mw (kDa)
PSD-95-mCherry
Blot: RFP
PSD-95 (wild-type)
Blot: PSD95
α-tubulin
β-actin
Blot: α-tubulin/β-actin
Blot: GFP
a/b = 0.845 (%) c/d = 0.727 (%)
E
CAG-mCherry
Syp targeting vector (EGFP)
(+/–) CBh-Cas9/U6-gRNA(Syp)
Syp-EGFP
Blot: GFP
Syp (wild-type)
Blot: Syp
mCherry
Blot: RFP
e/f = 1.04 (%) g/h = 1.10 (%)
F
CAG-EGFP + PSD-95 targeting vector (mCherry)
(–) CBh-Cas9/U6-gRNA (PSD-95)
(+) CBh-Cas9/U6-gRNA (PSD-95)
mCherry
GFP/mCherry/PSD-95
Cortical neurons (21 div)
Hippocampal neurons (21 div)
50 μm
G
Syp targeting vector (EGFP) + CAG-mCherry
(–) CBh-Cas9/U6-gRNA (Syp)
(+) CBh-Cas9/U6-gRNA (Syp)
EGFP
EGFP/mCherry/Syp
Cortical neurons (24 div)
Hippocampal neurons (24 div)
100 μm

constructed and introduced into primary neuron cultures together with the CRISPR constructs (Figure 2, A and F). Genomic PCR analysis and fluorescence microscopy showed that both EGFP and mCherry can be used to label endogenous PSD-95 and Syp in primary cultured neurons (Figure 2, B, C, I, and J; Supplemental Table S1). These data also demonstrate the flexibility of fluorescent tags, which is useful for multicolor imaging.

Morphological analysis of neurons expressing fluorescently tagged PSD-95

Dynamics of the synaptic structure in living neurons are usually visualized by transfecting cDNAs encoding fluorescent protein-tagged PSD-95. However, ectopic expression of fluorescently tagged target proteins by transfecting exogenous genes often causes overexpression and mistargeting of the proteins, and it is hard to reproduce the expression levels and patterns of target proteins faithfully. Overexpressed or aberrantly localized exogenous proteins sometimes cause undesirable side effects. Ectopic expression of fluorescent protein-tagged PSD-95 in neurons increases the number and size of dendritic spines, alters synaptic currents, and impairs synaptic plasticity (El-Husseini *et al.*, 2000; Béïque and Andrade, 2003; Stein *et al.*, 2003; Ehrlich and Malinow, 2004; Fortin *et al.*, 2014). Consistent with the previous reports, ectopic expression of a PSD-95-EGFP fusion protein in primary hippocampal neurons using the CAG promoter (Niwa *et al.*, 1991) caused enlarged spines (Figure 3, A and C). BDNF, a member of the neurotrophin family, is a critical factor that regulates synaptic development in the CNS (Poo, 2001). Treatment of hippocampal neurons with BDNF increases the synapse number and spine density in dendrites (Tyler and Pozzo-Miller, 2001; Ji *et al.*, 2005). However, ectopic expression of a PSD-95-EGFP fusion protein by itself induced a significant increase in spine density as reported previously (El-Husseini *et al.*, 2000), and treatment with BDNF did not change the density of spines (Figure 3, A and B).

In sharp contrast, neurons expressing endogenous PSD-95 tagged with EGFP by CRISPR/Cas9-mediated gene knock-in displayed the equivalent number and size of dendritic spines to those of mock-transfected control cells, and a significant increase in spine density was observed after exposure to BDNF (Figure 3, A–C). Enhanced immunoreactivity for endogenous PSD-95 protein in BDNF-treated neuronal culture has been reported (Jourdi *et al.*, 2003), and we observed BDNF-induced enhancement of PSD-95-EGFP fluorescence (Figure 3A). These results demonstrate the advantages of the CRISPR/Cas9-mediated gene knock-in system for fluorescent labeling of proteins whose overexpression influences cellular functions.

To investigate the molecular causes for altered synaptic morphology induced by ectopic expression of the synaptic proteins, we examined the effects of ectopic expression of PSD-95 on the expression of endogenous Syp, and ectopic expression of Syp on the expression of endogenous PSD-95. Ectopic expression of the EGFP fusion of a postsynaptic protein, PSD-95-EGFP, under the CAG promoter in primary hippocampal neurons induced up-regulation of the expression of an endogenous presynaptic protein, Syp (Figure 4A). Conversely, ectopic expression of the mCherry fusion of a presynaptic protein, Syp-mCherry, induced up-regulation of an endogenous postsynaptic protein, PSD-95 (Figure 4B). These data suggest that expression levels of the pre- and postsynaptic proteins mutually influence each other in neurons where the synaptic proteins are ectopically overexpressed.

We also performed the CRISPR/Cas9-mediated gene knock-out to examine the correlation of the expressions of endogenous Syp and PSD-95 proteins in cultured hippocampal neurons. As Cas9 target sites, four and three different target sites followed by the PAM sequences were chosen in the rat Syp and PSD-95 genes, respectively (Figure 5, A and C). Two of the prepared gRNAs for each gene were used in combination to achieve higher editing efficiency. We detected the CRISPR/Cas9-dependent induction of intended genomic deletions by PCR analysis of genomic DNA samples isolated from the cultures using the primer sets amplifying the Cas9 target regions (Figure 5, B and D). Targeted genome modifications were also verified by Sanger sequencing of the PCR amplicons (Supplemental Figures S3 and S4). Western blot analysis of whole-cell lysates from 3-wk-old neurons confirmed the CRISPR/Cas9-dependent reduction in Syp and PSD-95 protein expression (Figure 5, E and F). Moreover, in the presynaptic Syp and postsynaptic PSD-95 knock-out cultures, in which the expression of each targeted protein was suppressed, a corresponding decrease in the expression of postsynaptic PSD-95 and presynaptic Syp was observed. These results suggest that endogenous Syp and PSD-95 support the expression of each other during neuronal maturation.

FIGURE 1: Fluorescent tag knock-in in primary cultured rat neurons using a combined method of CRISPR/Cas9 genome-editing and nucleofection. (A) Schematic overview of the protocol for fluorescent tag knock-in in rat primary cortical and hippocampal neurons. (B) Structures of the rat *PSD-95* locus and the knock-in targeting vector to produce a PSD-95-mCherry fusion protein. The predicted Cas9-gRNA cutting positions are indicated with scissor-cutting symbols. (C) Structures of the rat *Syp* locus and the knock-in targeting vector to produce a Syp-EGFP fusion protein. The predicted Cas9-gRNA cutting positions are indicated with scissor-cutting symbols. (D, E) Western blot analysis of whole-cell lysates from 21 DIV rat primary cortical or hippocampal neurons nucleofected with the indicated plasmids. Immunoblots were probed with indicated antibodies. A PSD-95-mCherry fusion protein (~110 kDa) was detected only in the presence of CBh-Cas9/U6-gRNA (PSD-95), and a Syp-EGFP fusion protein (~65 kDa) was detected only in the presence of CBh-Cas9/U6-gRNA (Syp). Intensities of Western blot bands corresponding to tagged and wild-type PSD-95 (a, b and c, d) or Syp (e, f and g, h) were quantified by densitometric analysis, and the tagging efficiency (a/b, c/d, e/f, and g/h) were calculated and shown at the bottom. (F) Cortical (top panels) or hippocampal (bottom panels) neurons nucleofected with the indicated plasmids were cultured for 21 d. Fixed neurons were stained with anti-GFP (green), anti-mCherry (magenta in color panels, or black in black and white panels), and anti-PSD-95 (blue) antibodies. mCherry-positive cells were observed only in the presence of CBh-Cas9/U6-gRNA (PSD-95). Bar, 50 μm. Residual background signals observed in the mCherry channel were derived from nonspecific antibody staining background (see Supplemental Figure S2). (G) Cortical (top panels) or hippocampal (bottom panels) neurons nucleofected with the indicated plasmids were cultured for 21 d. Fixed neurons were stained with anti-GFP (green in color panels, or black in black and white panels), anti-mCherry (magenta), and anti-Syp (blue) antibodies. EGFP-positive cells were observed only in the presence of CBh-Cas9/U6-gRNA (Syp). Bar, 100 μm. Residual background signals observed in the GFP channel were derived from nonspecific antibody staining background (see Supplemental Figure S2).

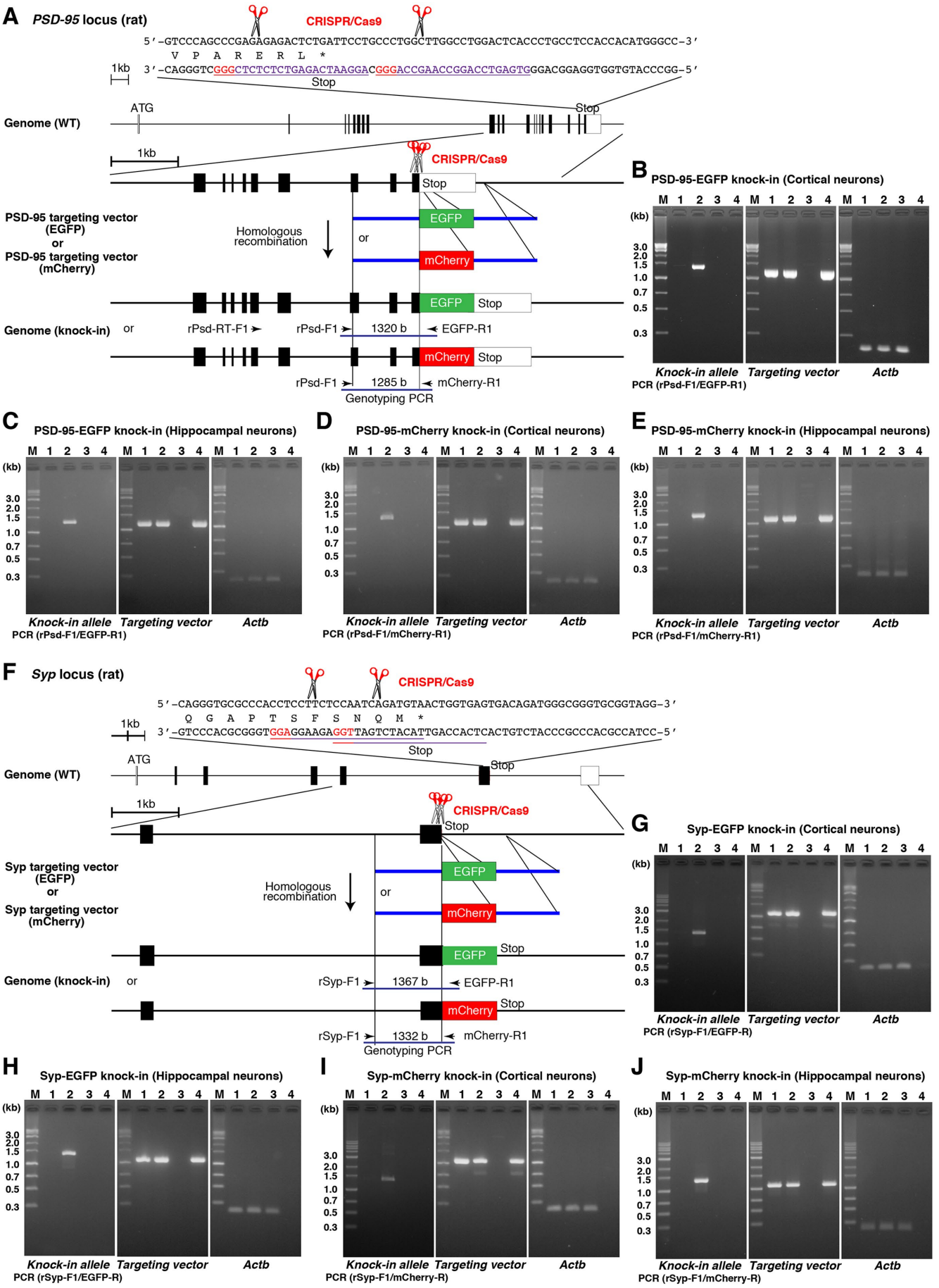
A PSD-95 locus (rat)
CRISPR/Cas9
5′-GTCCCAGCCCGAGAGAGACTCTGATTCCTGCCCTGGCTTGGCCTGGACTCACCCTGCCTCCACCACATGGGCC-3′
V P A R E R L *
1kb
3′-CAGGGTCGGGCTCTCTCTGAGACTAAGGACGGGACCGAACCGGACCTGAGTGGGACGGAGGTGGTGTACCCGG-5′
Stop
Stop
Genome (WT)
ATG
1kb
CRISPR/Cas9
Stop
PSD-95 targeting vector (EGFP) or PSD-95 targeting vector (mCherry)
Homologous recombination
or
EGFP
mCherry
EGFP
Stop
Genome (knock-in)
or
rPsd-RT-F1
rPsd-F1
1320 b
EGFP-R1
mCherry
Stop
rPsd-F1
1285 b
mCherry-R1
Genotyping PCR
B PSD-95-EGFP knock-in (Cortical neurons)
M 1 2 3 4 M 1 2 3 4 M 1 2 3 4
(kb)
3.0
2.0
1.5
1.0
0.7
0.5
0.3
Knock-in allele
Targeting vector
Actb
PCR (rPsd-F1/EGFP-R1)
C PSD-95-EGFP knock-in (Hippocampal neurons)
M 1 2 3 4 M 1 2 3 4 M 1 2 3 4
(kb)
3.0
2.0
1.5
1.0
0.7
0.5
0.3
Knock-in allele
Targeting vector
Actb
PCR (rPsd-F1/EGFP-R1)
D PSD-95-mCherry knock-in (Cortical neurons)
M 1 2 3 4 M 1 2 3 4 M 1 2 3 4
(kb)
3.0
2.0
1.5
1.0
0.7
0.5
0.3
Knock-in allele
Targeting vector
Actb
PCR (rPsd-F1/mCherry-R1)
E PSD-95-mCherry knock-in (Hippocampal neurons)
M 1 2 3 4 M 1 2 3 4 M 1 2 3 4
(kb)
3.0
2.0
1.5
1.0
0.7
0.5
0.3
Knock-in allele
Targeting vector
Actb
PCR (rPsd-F1/mCherry-R1)
F Syp locus (rat)
CRISPR/Cas9
5′-CAGGGTGCGCCCACCTCCTTCTCCAATCAGATGTAACTGGTGAGTGACAGATGGGCGGGTGCGGTAGG-3′
Q G A P T S F S N Q M *
1kb
3′-GTCCCACGCGGGTGGAGGAAGAGGTTAGTCTACATTGACCACTCACTGTCTACCCGCCCACGCCATCC-5′
Stop
Stop
Genome (WT)
ATG
1kb
CRISPR/Cas9
Stop
Syp targeting vector (EGFP) or Syp targeting vector (mCherry)
Homologous recombination
or
EGFP
mCherry
EGFP
Stop
Genome (knock-in)
or
rSyp-F1
1367 b
EGFP-R1
mCherry
Stop
rSyp-F1
1332 b
mCherry-R1
Genotyping PCR
G Syp-EGFP knock-in (Cortical neurons)
M 1 2 3 4 M 1 2 3 4 M 1 2 3 4
(kb)
3.0
2.0
1.5
1.0
0.7
0.5
0.3
Knock-in allele
Targeting vector
Actb
PCR (rSyp-F1/EGFP-R)
H Syp-EGFP knock-in (Hippocampal neurons)
M 1 2 3 4 M 1 2 3 4 M 1 2 3 4
(kb)
3.0
2.0
1.5
1.0
0.7
0.5
0.3
Knock-in allele
Targeting vector
Actb
PCR (rSyp-F1/EGFP-R)
I Syp-mCherry knock-in (Cortical neurons)
M 1 2 3 4 M 1 2 3 4 M 1 2 3 4
(kb)
3.0
2.0
1.5
1.0
0.7
0.5
0.3
Knock-in allele
Targeting vector
Actb
PCR (rSyp-F1/mCherry-R)
J Syp-mCherry knock-in (Hippocampal neurons)
M 1 2 3 4 M 1 2 3 4 M 1 2 3 4
(kb)
3.0
2.0
1.5
1.0
0.7
0.5
0.3
Knock-in allele
Targeting vector
Actb
PCR (rSyp-F1/mCherry-R)

Application of gene knock-in for monitoring transcriptional and translational changes

The early effects of BDNF on synapses result from the modifications of components already available at the synapse. These modifications include protein phosphorylation and accumulation. On the other hand, the long-term effects of BDNF require changes in transcription and modifications of translational activity at the synapse (Leal *et al.*, 2014). BDNF-TrkB signaling upregulates translational activity at the synapse, and BDNF treatment enhances the expression of both presynaptic and postsynaptic proteins, including synapsin I and PSD-95 (Cheng *et al.*, 2012). With the use of the fluorescent gene knock-in method, we observed an increase in the expression of EGFP-tagged endogenous PSD-95 protein in hippocampal neurons, following treatment with BDNF (Figure 6A).

Activity-dependent gene expression of *PSD-95* has also been reported (Bao *et al.*, 2004), and up-regulation of EGFP-tagged PSD-95 was observed at both protein and mRNA levels, as revealed by Western blot and reverse transcription-PCR (RT-PCR) analyses, after treatment of the cortical neurons with KCl that induces depolarization (Figure 6, B–D). These data show that the gene knock-in technique can be used to monitor the transcriptional and translational changes of target proteins at the synapses of cultured neurons.

Labeling multiple endogenous synaptic proteins within a single neuron

Multiplex labeling of pairs of pre- and postsynaptic proteins with different fluorescent proteins would enable high-resolution analysis of correlated localization of two different proteins within a single cell. Multiplex genome engineering using CRISPR/Cas9 has been reported (Cong *et al.*, 2013), and it has been recently reported that double labeling of two proteins in the same cell with nonfluorescent small tags of HA and FLAG is achieved in the mouse cerebral cortex in vivo (Mikuni *et al.*, 2016). We tried to colabel endogenous PSD-95 and Syp with mCherry and EGFP, respectively, in the same cell in primary cultures of rat hippocampal neurons. We performed cotransfection of dissociated neurons with the two targeting vectors, PSD-95 targeting vector (mCherry) and Syp targeting vector (EGFP), in the presence or absence of the CRISPR constructs (CBh-Cas9/U6-gRNAs) against *PSD-95* and *Syp*, using the nucleofection technology, and the cultures were fixed and immunostained at 15 DIV. A small number of EGFP and mCherry double-positive neurons, which underwent simultaneous knock-in of the fluorescent genes, was observed (Figure 7A).

Overexpression tends to cause artifacts of protein sorting, including aberrant subcellular localizations and erroneous formation of protein complexes. To determine whether overexpressions of PSD-95 and Syp affect their own subcellular localization patterns in neurons, we compared the localization of three types of PSD-95 and Syp proteins: endogenous ones immunofluorescently labeled with anti-PSD-95 and Syp antibodies, endogenous ones simultaneously tagged with EGFP and mCherry by CRISPR/Cas9-mediated gene knock-in, and ectopically expressed ones fused to EGFP and mCherry. We observed the subcellular localization patterns of PSD-95 and Syp proteins within a single cell using confocal laser scanning microscopy and found that endogenous PDS-95 and Syp detected using anti-PSD-95 and anti-Syp antibodies or tagged with fluorescent proteins using CRISPR/Cas9 exhibited nondiffuse, punctate localization patterns. In contrast with this, ectopically expressed PDS-95 and Syp fused to fluorescent proteins showed diffuse localization patterns and partially colocalized within the cell body and shafts and protrusions of nerve processes (Figure 7B). These ectopic localizations became more apparent by using superresolution microscopy, which enables the visualization of protein localizations with higher optical resolution than that of conventional microscopy (Figure 7C). Superresolution microscopy of a process of a single cell revealed that puncta of fluorescently tagged endogenous PSD-95 and Syp localized adjacent to each other, but their signals never overlap. Such localization patterns were comparable to those visualized with anti-PSD-95 and anti-Syp antibodies. By contrast, ectopically expressed fluorescent fusion proteins of PSD-95 and Syp showed partially overlapping and diffuse expression patterns.

One of the advantages of fluorescent labeling is that labeled proteins can be used for live-cell imaging to analyze spatiotemporal regulations of protein localization and function. We performed live-cell TIRF microscopy of a single neuron that underwent simultaneous knock-in of the EGFP and mCherry fluorescent genes into *PDS-95* and *Syp* loci, respectively. The microscope was equipped with a high-speed electron-multiplying charge-coupled device (EMCCD) digital camera, which is extremely sensitive to support high-dynamic-range and high-speed imaging of low-light

FIGURE 2: Validation of CRISPR/Cas9-mediated knock-in of fluorescent genes into cultured neurons. (A, F) Structures of the rat *PSD-95* (A) and *Syp* (F) loci and the knock-in constructs to produce EGFP and mCherry fusion proteins. The gRNA targeting sequences are underlined, and the PAM sequences are shown in red. The predicted Cas9-gRNA cutting positions are indicated with a scissor-cutting symbols. These two gRNAs for each gene were used together to increase the knock-in efficiency. Locations of genotyping primers sets to detect EGFP or mCherry knock-in alleles of *PSD-95* (EGFP: rPsd-F1 and EGFP-R1; mCherry: rPSD-F1 and mCherry-R1) and *Syp* (EGFP: rSyp-F1 and EGFP-R1; mCherry: rSyp-F1 and mCherry-R1) are shown. (B–E) Genomic PCR analysis of nucleofected neurons. Cortical (B, D) or hippocampal (C, E) neurons were nucleofected with three plasmids: PSD-95 targeting vector (EGFP), CAG-mCherry, and CBh-Cas9 with or without gRNAs for *PSD-95* (B, C), or PSD-95 targeting vector (mCherry), CAG-EGFP, and CBh-Cas9 with or without gRNAs for *PSD-95* (D, E). Genomic DNA samples extracted from the cultured neurons at 21 DIV were subjected to PCR analysis. PCR primer sets were used to detect the fluorescent protein knock-in alleles, transfected targeting vectors, and endogenous rat *Actb*, respectively. Agarose gel electrophoresis of PCR products are shown: lane 1, DNA prepared from the primary neuron cultures nucleofected without CBh-Cas9/U6-gRNA (PSD-95); lane 2, DNA prepared from the neuron primary cultures nucleofected with CBh-Cas9/U6-gRNA (PSD-95); lane 3, wild-type rat genomic DNA; lane 4, PSD-95 targeting vector plasmid DNA. (G–J) Genomic PCR analysis of nucleofected neurons. Cortical (G, I) or hippocampal (H, J) neurons were nucleofected with three plasmids: Syp targeting vector (EGFP), CAG-mCherry, and CBh-Cas9 with or without gRNAs for *Syp* (G, H), or Syp targeting vector (mCherry), CAG-EGFP, and CBh-Cas9 with or without gRNAs for *Syp* (I, J). Genomic DNA samples extracted from the cultured neurons at 21 DIV were subjected to PCR analysis. PCR primer sets were used to detect the fluorescent protein knock-in alleles, transfected targeting vectors, and endogenous rat *Actb*, respectively. Agarose gel electrophoresis of PCR products are shown: lane 1, DNA prepared from the primary neuron cultures nucleofected without CBh-Cas9/U6-gRNA (Syp); lane 2, DNA prepared from the neuron primary cultures nucleofected with CBh-Cas9/U6-gRNA (Syp); lane 3, wild-type rat genomic DNA; lane 4, Syp targeting vector plasmid DNA.

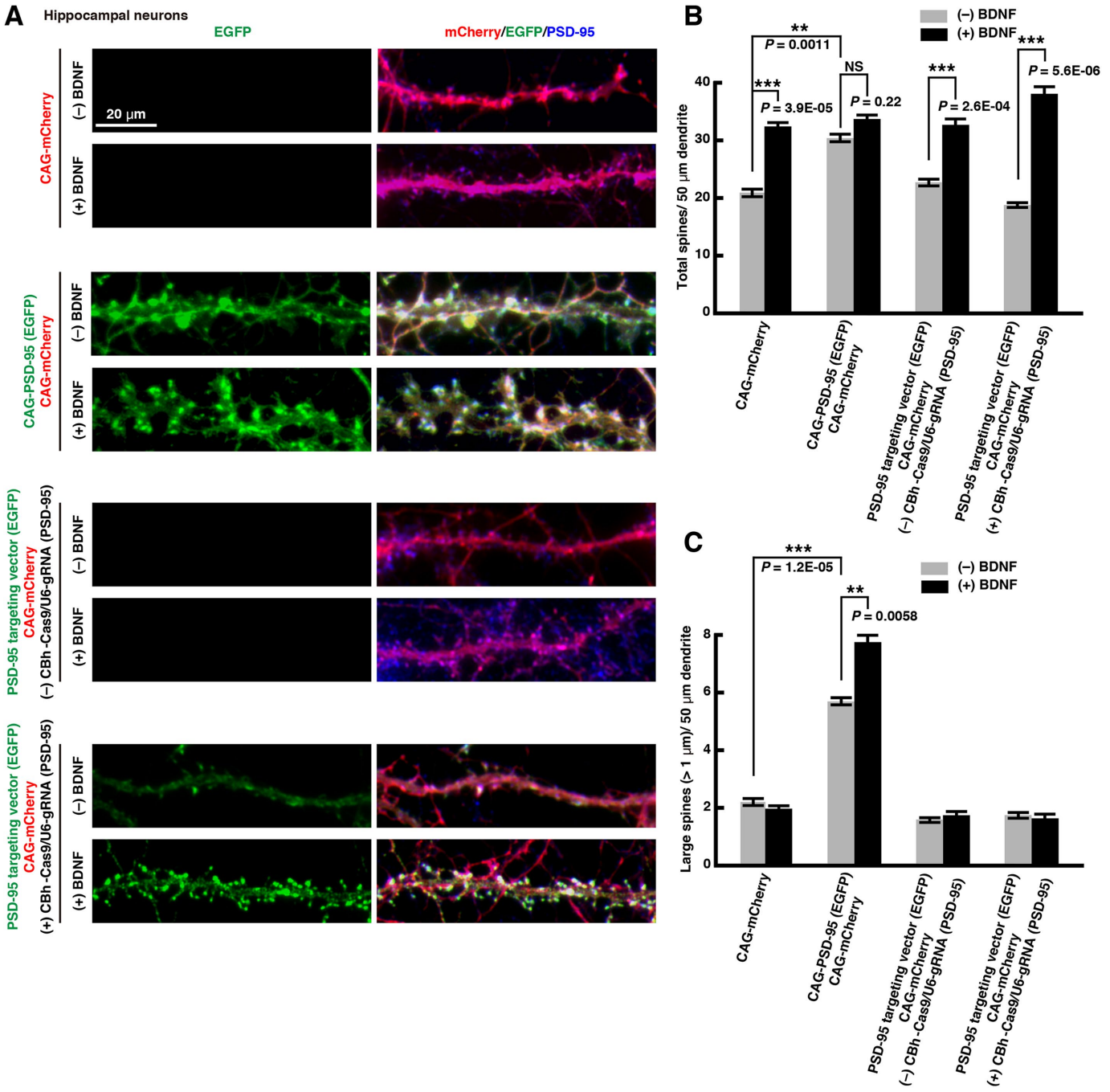

FIGURE 3: Morphological analysis of hippocampal neurons expressing fluorescently tagged PSD-95. (A) Primary cultured hippocampal neurons nucleofected with the indicated plasmid constructs were treated with BDNF (50 ng/ml) or the corresponding vehicle control for 1 d prior to fixation at 21 DIV. Fixed neurons were stained with anti-GFP (green), anti-mCherry (magenta), and anti-PSD-95 (blue) antibodies. Global morphology of dendrites is visualized by CAG-mCherry fluorescence. Bar, 20 μm. (B, C) Quantitative analysis of the numbers of dendritic spines in neurons in A. Dendritic spines were defined as <6 μm dendritic protrusions with mushroom-shaped heads or stubby-shaped structures as visualized by CAG-mCherry fluorescence. The numbers of total spines (B) and large spines (>1 μm width) (C) per 50 μm of dendrite segments are quantified; $n = 50$ (50 dendrite segments from 25 neurons); mean ± SEM (error bars); $^{**}p < 0.01$; $^{***}p < 0.001$; one-way ANOVA with Dunnett's post hoc test.

fluorescence of raw fluorescent signals of endogenously tagged proteins. With the system, we observed that puncta of PSD-95-EGFP and Syp-mCherry were localized along a process of a single neuron forming adjacent pairs (Figure 7D). We also revealed the previously undescribed synchronous and dynamic localization of the puncta of PSD-95-EGFP and Syp-mCherry along a process in response to BDNF stimulation (Figure 7D and Supplemental Video S1). Some PSD-95-EGFP positive puncta, which are considered to be dendritic spines, were produced after BDNF treatment, and the adjacent localization of EGFP and mCherry puncta was also observed even in the newly formed spines. These results demonstrate that CRISPR/Cas9-mediated fluorescent gene

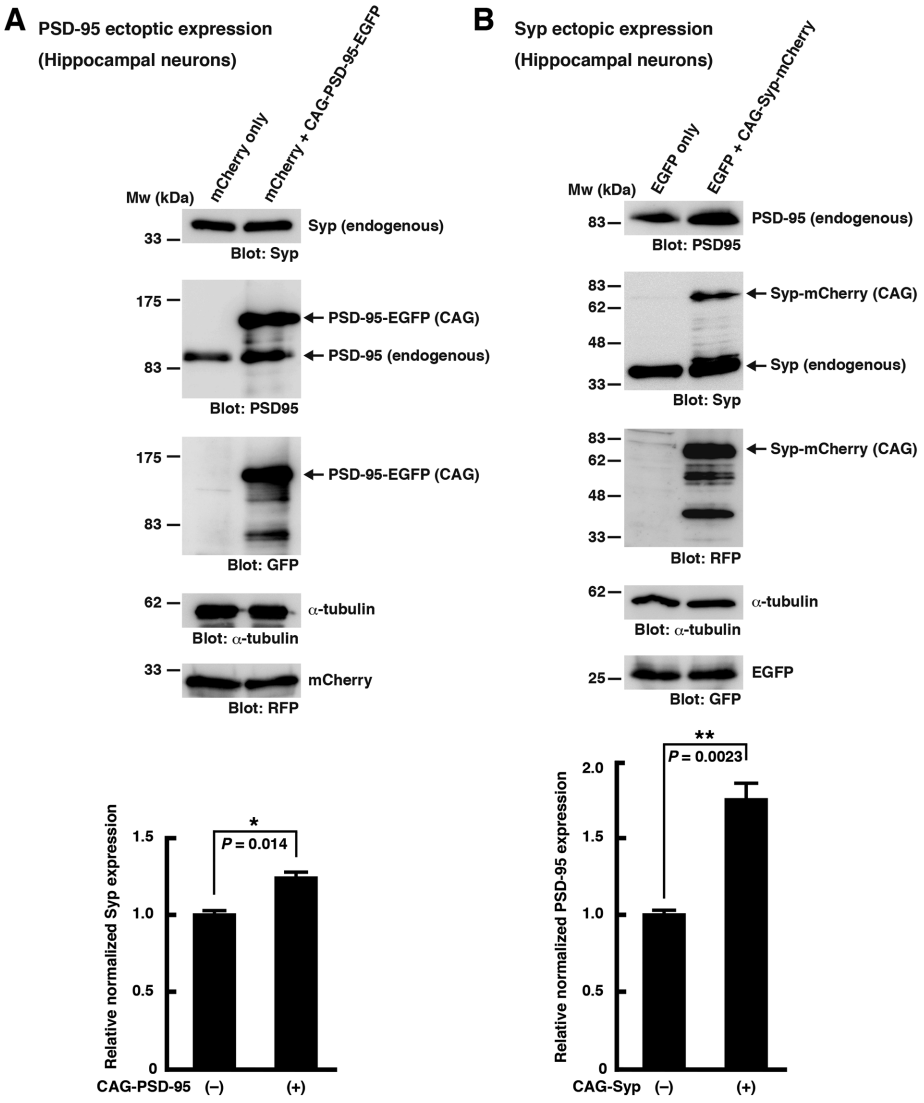

FIGURE 4: Correlations between expression levels of pre- and postsynaptic proteins in cultured neurons where synaptic proteins are ectopically overexpressed. (A) Western blot analysis of whole-cell lysates from 16 DIV rat primary hippocampal neurons nucleofected with CAG-mCherry alone or CAG-mCherry plus CAG-PSD-95-EGFP. Immunoblots were probed with indicated antibodies, and densitometric analysis of blots was performed to determine the fold differences in endogenous Syp expression. (B) Western blot analysis of whole-cell lysates from 16 DIV rat primary hippocampal neurons nucleofected with CAG-EGFP alone or CAG-EGFP plus CAG-Syp-mCherry. Immunoblots were probed with indicated antibodies, and densitometric analysis of blots was performed to determine the fold differences in endogenous PSD-95 expression. The graphs show quantitative densitometry and statistical analysis of the Western blot bands; $n = 3$ (three blot membranes from three sample sets); mean ± SEM (error bars); $*p < 0.05$; $**p < 0.01$; Student's t test. The relative expression levels of endogenous Syp and PSD-95 were normalized to the expression level of α-tubulin.

knock-in in primary cultured neurons enables monitoring of the dynamics of endogenous proteins in a living neuron at single-cell resolution, and that multiplex labeling of proteins with different fluorescent proteins facilitates high-resolution analysis of correlated localization of a pair of two different proteins.

DISCUSSION

In this study, we have developed a versatile, convenient, and nonviral method for analyzing the localization of endogenous proteins in individual neurons of complex neuronal networks. We succeeded in fluorescent tagging of endogenous synaptic proteins in cultured postmitotic neurons by the combined use of the CRISPR/Cas9 genome-editing technology with the nucleofection technique. Our method is particularly useful for analyzing the spatiotemporal localization of proteins whose ectopic overexpression induces aberrant localization and perturbs cellular functions. Moreover, the labeling method is ideal for imaging of neurons of highly complex neural networks since only a limited number of transfected cells undergo CRISPR/Cas9-mediated homologous recombination. With the method, we can also follow the synaptic stimuli-induced expression changes in both mRNA and protein levels.

Limitations of the fluorescent gene knock-in method

Overall, the method developed in this study can provide a high-throughput approach for examination of various endogenous proteins. However, there are a few limitations in this labeling method. The first limitation is that it is hard to analyze genomic structures of individual neurons prior to imaging and functional studies. Unlike cultured cell lines, which proliferate infinitely, or fertilized eggs, which develop into adult bodies through many cell divisions, primary cultured neurons do not clonally expand. Therefore, it is almost impossible to select the correctly targeted neurons verified by genotyping for subsequent analysis. In addition, cells with off-target mutations induced by the Cas9 nuclease cannot be excluded. To overcome these issues, we planned to develop a method to identify the correctly targeted neurons in dishes without genotyping and a strategy to minimize the unintended mutations in target genes. In this study, we employed the "C-terminal fusion approach" focusing on the fact that there is usually no promoter activity around the exons encoding the C-termini of proteins. We thought that knock-in targeting vectors carrying fluorescent reporters and the genomic DNAs encoding the C-terminal regions of proteins do not express fluorescent proteins by themselves, but that the fluorescent proteins are expressed on integration of the targeting vectors into the genome by CRISPR/Cas9-mediated homologous recombination. As expected, the C-terminal fusion approach worked well in primary cultured neurons with few false-positive signals. We did not see any evidence suggesting mistargeting or off-target events. Subcellular localization patterns of all the fluorescent signals we examined were identical to those of PSD-95 and Syp. Unexpectedly, we observed a very few EGFP- or mCherry-positive signals in neurons transfected with the knock-in donor plasmids even in the absence of the CRISPR constructs (Supplemental Table S1). Subcellular localization patterns of these fluorescent signals were also identical to those of PSD-95 and Syp. Moreover, we

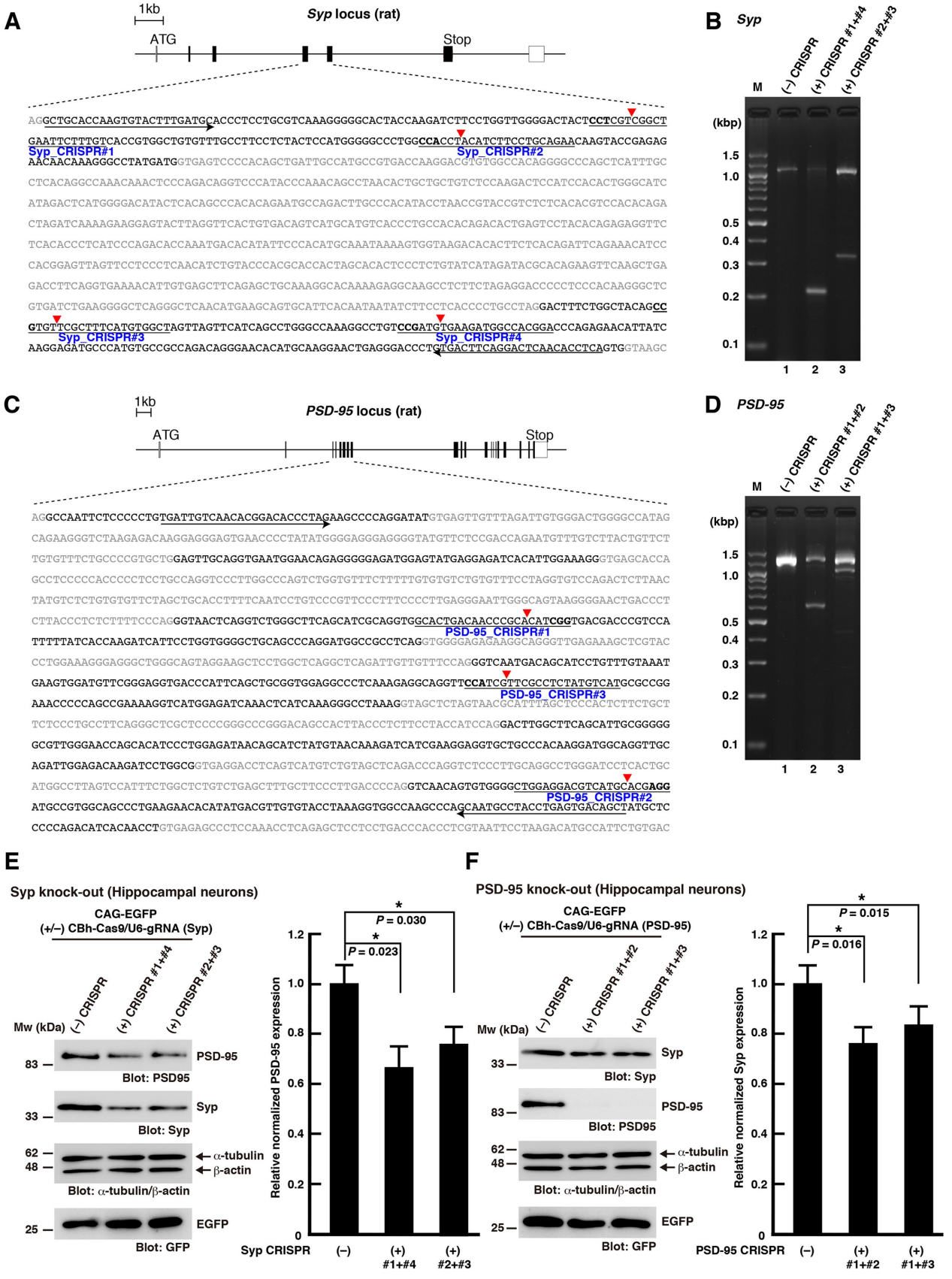

FIGURE 5: CRISPR/Cas9-mediated knock-out of *Syp* and *PSD-95* to examine the correlation of endogenous expression of pre- and postsynaptic proteins in cultured neurons. (A, C) The structure of the rat *Syp* locus and the nucleotide sequence of exon 4–5 (A), and the structure of rat *PSD-95* locus and the nucleotide sequence of exon 3–8 (C). Intron sequences are shown in gray. The gRNA targeting sequences are underlined, and the PAM sequences are shown in

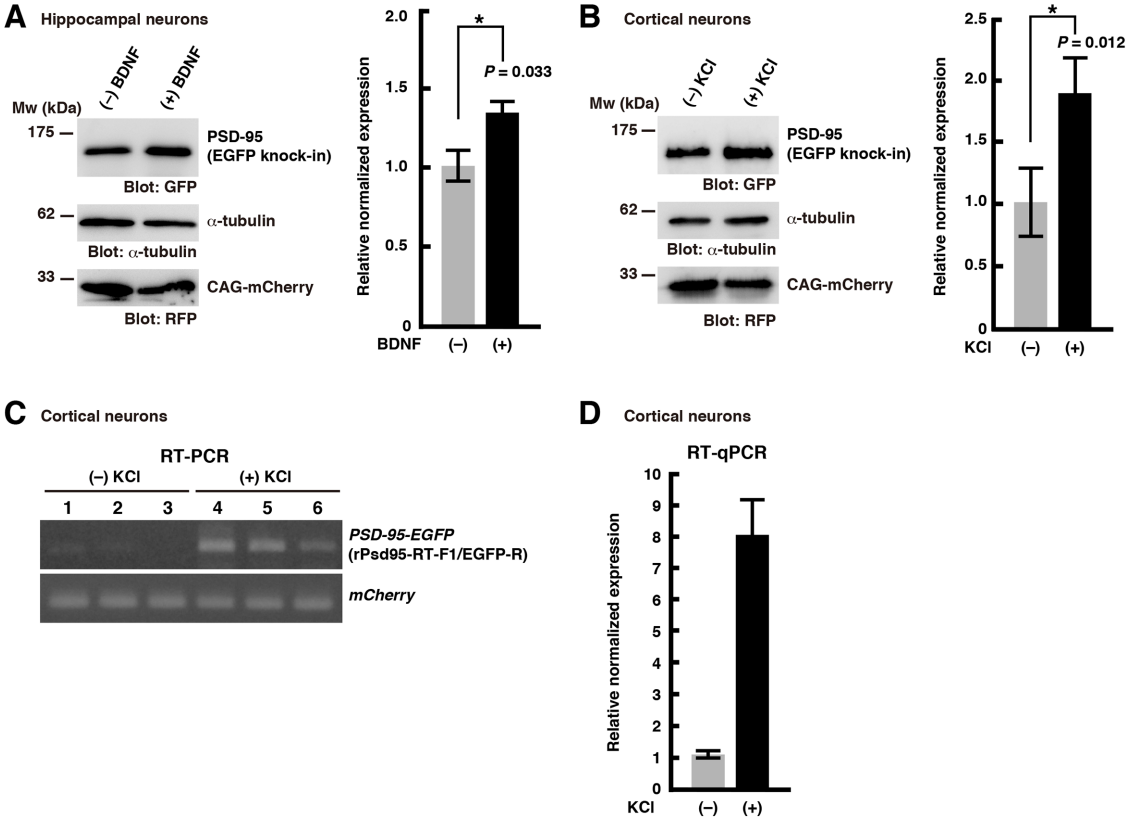

FIGURE 6: Application of CRISPR/Cas9-mediated fluorescent tag knock-in for monitoring transcriptional and translational expression changes. (A) Western blot analysis of whole-cell lysates from 21 DIV primary hippocampal neurons nucleofected with PSD-95 targeting vector (EGFP), CAG-mCherry, and CBh-Cas9/U6-gRNA (PSD-95), and treated with BDNF (50 ng/ml) or the corresponding vehicle control for 1 d prior to harvest. Immunoblots were probed with indicated antibodies, and densitometric analysis of blots was performed to determine the fold differences in endogenous PSD-95 protein expression tagged with EGFP. (B) Western blot analysis of whole-cell lysates from 16 DIV primary cortical neurons nucleofected with PSD-95 targeting vector (EGFP), CAG-mCherry, and CBh-Cas9/U6-gRNA (PSD-95), and treated with 20 mM KCl or the corresponding vehicle control for 15 min at 15 DIV. Immunoblots were probed with indicated antibodies, and densitometric analysis of blots was performed to determine the fold differences in endogenous PSD-95 protein expression tagged with EGFP. The graphs show quantitative densitometry and statistical analysis of the Western blot bands; $n = 3$ (3 blot membranes from 3 sample sets); mean ± SEM (error bars); $*p < 0.05$; Student's *t* test. The relative expression level of endogenous PSD-95 tagged with EGFP was normalized to that of α-tubulin. (C, D) Cortical neurons nucleofected with PSD-95 targeting vector (EGFP), CAG-mCherry, and CBh-Cas9/U6-gRNAs (PSD-95), and treated with or without 20 mM KCl for 15 min at 15 DIV were subjected to RT-PCR analysis (C) or quantitative RT-PCR analysis (D) at 16 DIV. Primer sets were designed to detect cDNAs of *PSD-95-EGFP* expressed from a knock-in allele, and *mCherry* from CAG-mCherry served as the transfection control. Six independently prepared cultures were analyzed. The graph represents mean ± SEM (error bars), $n = 3$ (three sample sets). The relative expression level of endogenous *PSD-95* tagged with *EGFP* was normalized to that of *mCherry*.

bold. The predicted Cas9-gRNA cutting positions are indicated with red triangles. Arrows denote the position of the PCR primers used for genotyping. (B, D) Genomic PCR analysis of primary neuronal cultures nucleofected with the CRISPR constructs. Primary hippocampal neurons were nucleofected with CAG-EGFP and the following plasmids: CBh-Cas9 without gRNA (B and D, lane 1), a combination of CBh-Cas9/U6-gRNA (Syp#1) and CBh-Cas9/U6-gRNA (Syp#4) (B, lane 2), a combination of CBh-Cas9/U6-gRNA (Syp#2) and CBh-Cas9/U6-gRNA (Syp#3) (B, lane 3), a combination of CBh-Cas9/U6-gRNA (PSD-95#1) and CBh-Cas9/U6-gRNA (PSD-95#2) (D, lane 2), or a combination of CBh-Cas9/U6-gRNA (PSD-95#1) and CBh-Cas9/U6-gRNA (PSD-95#3) (D, lane 3). DNAs were extracted from the cultured neurons at 19 DIV and subjected to PCR analysis. Targeted genome modifications were also verified by Sanger sequencing of the PCR amplicons (see Supplemental Figures S3 and S4). (E, F) Western blot analysis of whole-cell lysates from 19 DIV rat primary hippocampal neurons nucleofected with the indicated CRISPR constructs. Immunoblots were probed with indicated antibodies, and densitometric analysis of blots was performed to determine the fold differences in endogenous expression of PSD-95 (E) or Syp (F). The graphs show quantitative densitometry and statistical analysis of the Western blot bands; $n = 3$ (three blot membranes from three sample sets); mean ± SEM (error bars); $*p < 0.05$; Student's *t* test. The relative expression levels of endogenous Syp and PSD-95 were normalized to the expression level of α-tubulin.

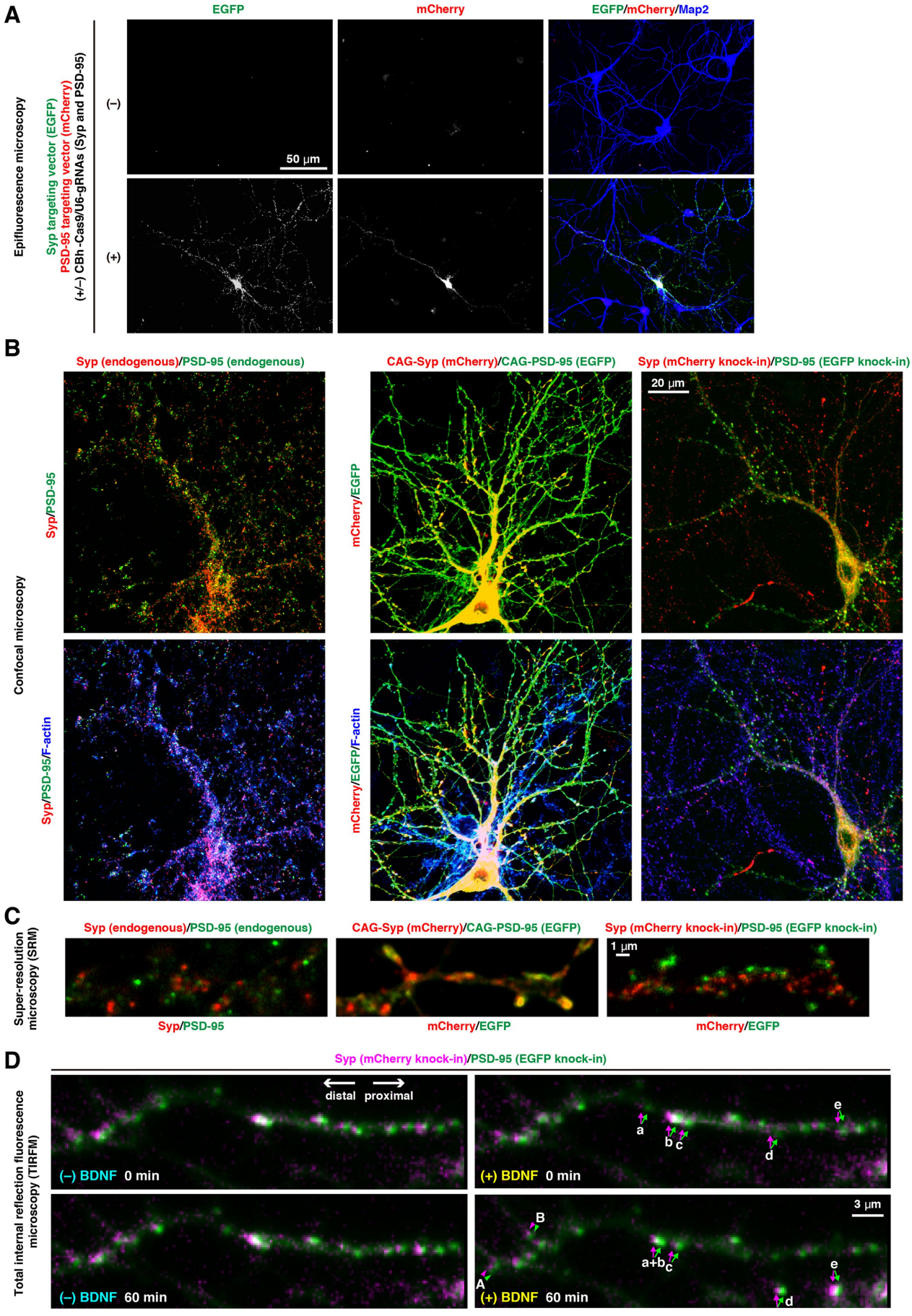
A
EGFP
mCherry
EGFP/mCherry/Map2
Epifluorescence microscopy
Syp targeting vector (EGFP)
PSD-95 targeting vector (mCherry)
(+/−) CBh -Cas9/U6-gRNAs (Syp and PSD-95)
(−)
(+)
50 μm
B
Syp (endogenous)/PSD-95 (endogenous)
CAG-Syp (mCherry)/CAG-PSD-95 (EGFP)
Syp (mCherry knock-in)/PSD-95 (EGFP knock-in)
Confocal microscopy
Syp/PSD-95
mCherry/EGFP
Syp/PSD-95/F-actin
mCherry/EGFP/F-actin
20 μm
C
Super-resolution microscopy (SRM)
Syp (endogenous)/PSD-95 (endogenous)
CAG-Syp (mCherry)/CAG-PSD-95 (EGFP)
Syp (mCherry knock-in)/PSD-95 (EGFP knock-in)
1 μm
Syp/PSD-95
mCherry/EGFP
mCherry/EGFP
D
Syp (mCherry knock-in)/PSD-95 (EGFP knock-in)
Total internal reflection fluorescence microscopy (TIRFM)
distal
proximal
(−) BDNF 0 min
(+) BDNF 0 min
(−) BDNF 60 min
(+) BDNF 60 min
a
b
c
d
e
A
B
a+b
c
3 μm

detected the knock-in alleles by PCR with higher numbers of cycles in the genomic DNA samples prepared from the neurons transfected with the knock-in donor plasmid without the CRISPR constructs. We speculate that they are not the cells to which the knock-in vectors were randomly integrated into the genome, but the cells in which spontaneous homologous recombination occurred without CRISPR/Cas9. It was previously reported that spontaneous homologous recombination generally occurs at a frequency of one event per 10^5–10^7 transfected cells, and that direct microinjection of donor plasmids into cells markedly increased the efficiency of homologous recombination (Vasquez *et al.*, 2001). Considering that the knock-in donor plasmids were introduced into neurons by nucleofection, which enables the DNA to enter directly into the nucleus, it is reasonable to see some neurons that underwent spontaneous gene knock-in without CRISPR/Cas9 under our experimental conditions.

In contrast to the C-terminal fusion approach, when a targeting vector is designed for N-terminal tagging, there is a high probability that the promoter region is included in the homology arm of the targeting vector (The ENCODE Project Consortium, 2012). In that case, the targeting vector would express a fluorescent reporter independently of CRISPR/Cas9-mediated homologous recombination, and it becomes hard to distinguish the true signals derived from fluorescent protein-tagged endogenous proteins. The C-terminal fusion approach is also beneficial to reduce the risk of unintended mutations in target genes in neurons that has undergone homologous recombination in only one of the two alleles for each gene, or in neurons that have not undergone gene knock-in. The Cas9 nuclease might induce unintended sequence changes through indel mutations mediated by NHEJ in the transfected cells if HDR does not occur. This problem matters particularly in the case of N-terminal tagging since altered sequence near the N-terminal region can change the transcription and translation of the target gene. On the other hand, in the case of C-terminal tagging, such a risk is relatively low.

The second limitation of this labeling technique is that fluorescent signal intensity may not be high enough for live-cell imaging in cases where the expression levels of target proteins are low. We acquired raw fluorescent images of fluorescently tagged endogenous synaptic proteins with a TIRF microscope equipped with an EMCCD digital camera, which is extremely sensitive to support high-dynamic-range and high-speed imaging of low-light fluorescence of raw fluorescent signals. Using our imaging system, we could readily conduct time-lapse imaging of endogenous PSD-95 and Syp in neurons. Generally, successful live-cell imaging of endogenous synaptic proteins depends on the copy numbers of target proteins. Previous reports estimated the number of PSD-95 molecules in single synapses to be ~300 (Chen *et al.*, 2005; Sugiyama *et al.*, 2005). Therefore, if the copy number of a target protein is comparable to or more than that of PSD-95, our technique should be sufficient for live-cell imaging. However, if the copy number of a target protein is much lower than that of PSD-95 (e.g., only a few copies per synapse), it may be difficult to conduct time-lapse imaging. With the development of more sensitive fluorescence detection systems and brighter fluorescent proteins, the method will become a more powerful and universal tool for monitoring the expression, localization, and functional dynamics of endogenous proteins.

The third limitation is that the knock-in efficiency is relatively low. The efficiency of fluorescent tag knock-in in primary cultured neurons was around or less than 1% for tagging of *PSD-95* and *Syp* (Supplemental Table S1). Such a low efficiency is usually enough and rather convenient for analysis of the protein of interest at single-cell resolution, and we managed to observe multiplexed labeling of a pre- and postsynaptic pairs of two proteins within a single cell, albeit scarcely. However, when we intend to perform multiplexed genetic labeling of three or more proteins, greater efficiency will be required.

In the present study, to increase the efficiency, we have made the following efforts. First, we have maximized transfection efficiency of postmitotic cells, including primary cortical and hippocampal neurons, by using the nucleofection technology, a modified form of electroporation that enables neuron-specific transfection with very high transfection efficiencies of up to 95% and with relatively low cell toxicity (Karra and Dahm, 2010; Matsuda *et al.*, 2019). Virus-based transfection methods have also been shown to be efficient, but they lack versatility in that they are often labor-intensive and time-consuming, and viral vectors have limitations of insert size. We tried lipid-mediated gene delivery using Lipofectamine2000 transfection reagent, whose efficiency is ~ 20–25% in the cortical neurons and 25–30% in the hippocampal neurons (Ohki *et al.*, 2001), but we failed to observe fluorescent cells that underwent genomic knock-in of fluorescent genes. We suppose that an inability of Lipofectamine2000 to achieve gene knock-in in primary neurons is due

FIGURE 7: Multiplex labeling of endogenous PSD-95 and Syp with fluorescent reporters in a single neuron. (A) Primary cultured hippocampal neurons nucleofected with Syp targeting vector (EGFP), PSD-95 targeting vector (mCherry), CBh-Cas9/gRNA (Syp), and CBh-Cas9/gRNA (PSD-95) were fixed at 21 DIV and stained with anti-GFP, anti-mCherry, and anti-MAP2 (blue; somatodendritic marker) antibodies. With epifluorescence microscopy, a small number of EGFP and mCherry double-positive neurons were observed. Bar, 50 µm. (B) Localizations of fluorescently labeled Syp and PSD-95 proteins within a single neuron of primary cultured hippocampal neurons at 21 DIV. Immunofluorescently labeled endogenous ones (left panels), ectopically expressed ones in a single neuron nucleofected with CAG-Syp-mCherry and CAG-PSD-95-EGFP (middle panels), and genetically labeled endogenous ones in a single neuron nucleofected with Syp targeting vector (mCherry), PSD-95 targeting vector (EGFP), CBh-Cas9/gRNAs (Syp), and CBh-Cas9/gRNAs (PSD-95) (right panels) were observed with confocal laser scanning microscopy. Fixed cells were stained with anti-PSD-95 (green) and anti-Syp (red) antibodies (left panels) or anti-GFP (green) and anti-mCherry (red) antibodies (middle and right panels). F-actin was stained with Alexa-647–conjugated phalloidin to visualize neuronal morphology (blue). Bar, 20 µm. (C) Dual-color superresolution microscopy of a primary cultured hippocampal neuron to observe protein localization of Syp (red) and PSD-95 (green) within a single process. Bar, 1 µm. (D) Live-cell TIRF microscopy of a single hippocampal neuron that underwent simultaneous knock-in of the EGFP and mCherry fluorescent genes into *PSD-95* and *Syp* loci, respectively. Images were acquired every 3 min starting from 1 h before until 1 h after the onset of 50 ng/ml BDNF application. See Supplemental Video S1. Images of a single process at the starting time of the video ((–) BDNF 0 min), at 1 h ((–) BDNF 60 min), at the onset of the BDNF application ((+) BDNF 0 min), and at 1 h after the BDNF application ((+) BDNF 60 min) are shown. Arrows indicate distal and proximal directions of a process. Newly formed fluorescent puncta emerged after BDNF treatment are labeled with arrowheads and capital letters, and preexisting puncta before BDNF treatment are labeled with arrows and small letters. Bar, 3 µm.

to its route of plasmid DNA delivery; the lipofectamine–plasmid DNA complex is released into the cytosol after being incorporated into a cell, whereas nucleofection enables direct delivery of the plasmid DNAs into the nucleus through the nuclear membrane independently of cell proliferation (Distler *et al.*, 2005; Karra and Dahm, 2010).

As the second approach to increase the knock-in efficiency, we prepared two gRNAs for each of the *PSD-95* and *Syp* genes and used together to achieve higher editing efficiency. We failed to obtain fluorescence gene knock-in neurons unless we used two gRNAs simultaneously for each gene. A similar approach has been used by other groups to increase the knock-in efficiency in mouse fertilized eggs and mouse ES cells (Zhou *et al.*, 2014; Acosta *et al.*, 2018; Jang *et al.*, 2018), though the mechanism underlying the enhance knock-in efficiency by two gRNAs is unknown. Given the fact that simultaneous use of two gRNAs exhibited much higher DNA cleavage activity compared with a single gRNA (Zhou *et al.*, 2014; Acosta *et al.*, 2018), two gRNAs may ensure cleavage of target genome and thereby enhance the knock-in efficiency. It was reported that genetic or pharmacological inhibition of the NHEJ pathway increases the HDR efficiency in mammalian cell lines (Chu *et al.*, 2015; Maruyama *et al.*, 2015). Inhibition of NHEJ may further increase the knock-in efficiency in primary cultured neurons.

Single-cell labeling of synaptic proteins

Dendritic spines are tiny protrusions of dendritic shafts that receive excitatory synaptic input and compartmentalize postsynaptic responses. Live-cell imaging studies have revealed that spines are remarkably dynamic, changing the size and shape over timescales of seconds to minutes (Hering and Sheng, 2001). Alterations in the density and morphology of dendritic spines have been proposed to enable persistent, long-term modifications of synapses and are characteristic of multiple cognitive disorders. Thus, elucidating the molecular mechanisms underlying spine alterations is important for understanding brain function. In this study, we could visualize the dendritic spines of primary cultured neurons by fluorescent labeling of endogenous PSD-95 and Syp with the use of the CRISPR/Cas9-mediated knock-in approach. It was reported that various endogenous proteins in the mouse brain can be labeled with the small epitope tags, such as HA and FLAG, using the similar approach. But in the case of PSD-95, the researchers failed to detect the epitope by immunostaining of the mouse brain in which the HA-tag was inserted to the C-terminus of PSD-95, although they confirmed the correct knock-in at the genomic level (Mikuni *et al.*, 2016). They speculated that this is likely due to inaccessibility of the antibody because of high protein density of PSD. In the present study, we have succeeded in observing raw fluorescent signals of endogenously tagged PSD-95 by fusing a fluorescent protein tag to the C-terminus of PSD-95 via a flexible linker of Gly and Ser-rich sequences (Supplemental Table S2). The fluorescent tags fused to PSD-95 are also detectable in fixed cells with conventional fluorescence microscopy after signal amplification by immunostaining with anti-fluorescent protein antibodies.

Dynamics of synaptic structure in living neurons are conventionally visualized by transfecting cDNAs encoding fluorescent protein-tagged PSD-95. This approach has been used by many researchers. However, ectopic overexpression of fluorescent protein-tagged PSD-95 in neurons by itself increases the number and size of dendritic spines, alters synaptic currents, and impairs synaptic plasticity (El-Husseini *et al.*, 2000; Béïque and Andrade, 2003; Stein *et al.*, 2003; Ehrlich and Malinow, 2004; Fortin *et al.*, 2014). For this reason, PSD-95 is considered as an example of difficult proteins to analyze the dynamic localization under physiological conditions in neurons. In the present study, we found that ectopic overexpression of a PSD-95-EGFP fusion protein in primary hippocampal neurons using the CAG promoter indeed caused enlargement of spines, while endogenous PSD-95 fused to EGFP did not change the number and size of dendritic spines. Our method would provide a high-throughput approach for examination of various endogenous synaptic proteins, including difficult proteins whose ectopic expression perturbs cellular functions.

The physiological relevance of correlated localization of Syp and PSD-95 puncta

Multiplex labeling of pre- and postsynaptic pairs of proteins with different fluorescent proteins enables high-resolution analysis of correlated localization of two different proteins within a single cell. With the CRISPR/Cas9-dependent system, we obtained neurons that underwent multiplex labeling of presynaptic Syp and postsynaptic PDS-95 within a single cell, albeit scarcely and only a single cell in the microscope field of view. The scarcity is convenient for observing the dynamics of endogenous proteins in a single neuronal process of complex neuronal networks. We observed that fluorescently tagged puncta of Syp and PSD-95 were localized forming adjacent pairs along a dendritic process of a single neuron, and we could monitor the previously undescribed synchronous and dynamic localization of the puncta of Syp and PSD-95 along a dendritic process in response to BDNF stimulation. Some PSD-95-positive small protrusions, which are considered to be dendritic spines, emerged after BDNF treatment, and the adjacent localization of PSD-95 and Syp was also observed even within the newly formed spines.

Syp is an integral membrane glycoprotein of synaptic vesicle providing pools of membranes, and a previous study of immunofluorescence labeling of cultured hippocampal neurons showed that Syp protein was localized throughout the neuron, and immunoreactivity could be seen not only in axons but also in cell bodies and dendrites (Cameron *et al.*, 1991). By immunofluorescent analyses, they also found the overlapping localization of Syp and transferrin receptors, which are markers for early endosomes during the process of endosomal membrane recycling, in the dendrites of hippocampal neurons in primary cultures before synapse formation. Axons were reported to be enriched in Syp immunoreactivity but did not contain detectable levels of transferrin receptor immunoreactivity. These reports suggest a novel role for dendritic Syp during synapse formation. It is possible that Syp participates in membrane recycling during membrane biogenesis of dendrites to form protrusions of future spines. However, distinct from a well-studied role of Syp as a presynaptic vesicle protein in axonal terminals, physiological relevance of dendritic localization of Syp has been unrevealed. Through a series of overexpression (Figure 4) and knock-out (Figure 5) studies of Syp and PSD-95 in cultured neurons, we revealed that Syp and PSD-95 support the expression of each other during neuronal maturation. Live-cell imaging of a single dendritic process revealed that some fluorescently tagged puncta of Syp and PSD-95 were localized forming adjacent pairs along a dendritic process of a single neuron. Previous work showed that the ubiquitin-proteasome pathway regulates protein stability of PSD-95, and PSD-95 protein is degraded by 26S proteasome following NMDA stimulation (Colledge *et al.*, 2003). We infer that PSD-95 puncta adjacently localized to Syp puncta are protected from the ubiquitin-proteasome machinery. Further studies will be required to clarify molecular mechanisms that contribute to the formation and stabilization of synaptic puncta in the process of synapse formation during brain development.

MATERIALS AND METHODS

Animal experiments

All animal experiments were approved by the Institutional Animal Care and Use Committee at the University of Hyogo and Kyoto University and conducted according to their guidelines. All procedures were performed in full compliance with the Fundamental Guidelines for Proper Conduct of Animal Experiments and Related Activities in Academic Research Institutions issued by the Japanese Ministry of Education, Culture, Sports, Science and Technology. Mice were housed under temperature-controlled conditions (temperature: 24°C) and maintained on a light/dark cycle (12 h each) with ad libitum access to food and water. Timed pregnant Wistar/ST rats were purchased from Japan SLC (Shizuoka, Japan).

Expression vectors

pCAG-EGFP (Addgene, #11150) has been described previously (Matsuda and Cepko, 2004). pCAG-mCherry was constructed by inserting the coding region of mCherry excised from pmCherry-N1 (Clontech) with *Eco*RI and *Not*I into pCAGEN (Addgene, #11160) digested with *Eco*RI and *Not*I. To construct pCAG-PSD-95-EGFP, the coding region of mouse *PSD-95* was obtained by RT-PCR from adult ICR mouse retina, using primers (5′-ATATCTCGAG-CTGAGCCGCCACCATGGACTGTCTCTGTATAGTGACAAC-3′ and 5′-AATTACCGGTGGATCCGAGTCTCTCTCGGGCTGGGAC-CCAGAT-3′). Linker-EGFP sequence was generated by PCR using primers (5′- CTCGGATCCACCGGTAATTCCGCTGACGGCGGCG-GAGGATCGGGTGGTAGTGGTGGTTCAGGAGGAGGATC-GACCCAAGGAGGTACCGTGAGCAAGGGCGAGGAGCTGTT-3′ and 5′-ATGCGCGGCCGCTTTACTTGTACAGCTC-3′) and pCAG-EGFP as a template. These PCR fragments were digested with *Xho*I and *Age*I, *Age*I and *Not*I, respectively, and simultaneously cloned into pCAGEN digested with *Xho*I and *Not*I. To construct pCAG-Syp-EGFP, the coding region of mouse *Syp* was amplified by RT-PCR from ICR mouse retina using primers (5′-ATATCTCGAG CTGAGCCGCCACCATGCTGCTGCTGGCAGACATGGAC-3′ and 5′-CGGTGGATCCGGAGAAGGAGGTGGGCGCACCCTGT-3′). Linker-EGFP sequence was generated by PCR using primers (5′-ACTCGGATCCACCGGTAATTCCGCTGACGGCG-3′ and 5′-AT-GCGCGGCCGCTTTACTTGTACAGCTC-3′) and pCAG-PSD95-EGFP as a template. These PCR fragments were digested with *Xho*I and *Bam*HI, *Bam*HI, and *Not*I, respectively, and simultaneously cloned into pCAGEN digested with *Xho*I and *Not*I. To construct pCAG-Syp-mCherry, pCAG-Syp-EGFP was digested with *Kpn*I and *Not*I, and the coding region of EGFP was replaced with that of mCherry amplified by PCR using primers (5′-ATATGGTACCGTGAGCAAGGGCGAGGAGGATAAC-3′ and 5′-GAGTGCGGCCGCTTTACTTGTACAG-3′) and pCAG-mCherry as a template, and digested with *Kpn*I/*Not*I.

The restriction enzyme sites are underlined.

CRISPR constructs

The CRISPR target sequences, 19-nucleotide sequence followed by a protospacer adjacent motif (PAM) of (5′-NGG-3′), were selected by using the prediction software (Doench *et al.*, 2014 www .broadinstitute.org/rnai/public/analysis-tools/sgrna-design). To create plasmids coexpressing *Streptococcus pyogenes* Cas9 and gRNA, following synthetic oligonucleotides were annealed and cloned into the *Bbs*I sites of pX330 (Cong *et al.*, 2013; Addgene, #42230). *PSD-95*; (5′-CACCGGTGAGTCCAGGCCAAGCCA-3′ and 5′-AAACTGGCTTGGCCTGGACTCACC-3′), (5′-CACCGAGGAAT-CAGAGTCTCTCTC-3′ and 5′-AAACGAGAGAGACTCTGATTC-CTC-3′), (5′-CACCGATGACATAGAGGCGAACGA-3′ and 5′-AAA-CTCGTTCGCCTCTATGTCATC-3′), (5′-CACCGGCACTGACAACC-CGCACAT-3′ and 5′-AAACATGTGCGGGTTGTCAGTGCC-3′), (5′-CACCGCTGGAGGACGTCATGCACG-3′ and 5′-AAACCGTG-CATGACGTCCTCCAGC-3′). *Syp*; (5′-CACCGTACATCTGATTG-GAGAAGG-3′ and 5′-AAACCCTTCTCCAATCAGATGTAC-3′), (5′-CACCGTCACCAGATTACATCTGAT-3′ and 5′-AAACATCAG-ATGTAATCTGGTGAC-3′), (5′-CACCGAGCCACATGAAAGCGAA CA-3′ and 5′-AAACTGTTCGCTTTCATGTGGCTC-3′), (5′-CACC-GTCCGTGGCCATCTTCACAT-3′ and 5′-AAACATGTGAAGATGGC-CACGGAC-3′), (5′-CACCGACAAAGAATTCAGCCGACG-3′ and 5′-AAACCGTCGGCTGAATTCTTTGTC-3′), (5′-CACCGTTCTGCAG-GAAGATGTAGG-3′ and 5′-AAACCCTACATCTTCCTGCAGAAC-3′). CRISPR constructs used in this study are listed in Supplemental Table S3.

Knock-in targeting vectors

To construct PSD-95 targeting vector (EGFP), the genomic DNA (1.9 kb) including exon 20 of rat *PSD-95* was amplified by PCR using primers (5′-CCATTTAAATGTCGACGGGAAGCACTGCATCCTC-GATGTC-3′ and 5′-GATCTTAATTAAGCTTCCGACCTGTGTCTCTC-CATTCCC-3′) and Wistar/ST rat genomic DNA as a template. The PCR fragment was digested with *Sal*I and *Hin*dIII and ligated into the pUC plasmid backbone amplified by PCR using pCAG-EGFP as a template, to generate pUC-rat PSD-95 genomic DNA. Then PCR was performed using primers (5′-AAATGCTAAGCGGCCGCCTG-GACTCACCCTGCCTCCAC-3′ and 5′-AATTACCGGTGGATCC-GAGTCTCTCTCGGGCTGGGAC-3′) and pUC-rat PSD-95 genomic DNA as a template. The PCR fragment was ligated with linker-EGFP excised from pCAG-PSD-95-EGFP with *Bam*HI and *Not*I, using the In-Fusion HD Cloning Kit (Takara Bio, Shiga, Japan) to generate PSD-95 targeting vector (EGFP). PSD-95 targeting vector (mCherry) was constructed by digesting PSD-95 targeting vector (EGFP) with *Bam*HI and *Not*I, and replacing the coding region of EGFP with that of mCherry excised from pCAG-Syp-mCherry with *Bam*HI/*Not*I.

To construct Syp targeting vector (EGFP), the genomic DNA (1.9 kb) including exon 6 of rat *Syp* was amplified by PCR using primers (5′-ATCGCTCGAG TTGAGACAGGGTCTACTTATATAGC-3′ and 5′-ATATAGATCT CGCTGGGTGGCAAAACAGGTTGTA-3′) and Wistar/ST rat genomic DNA as a template. The PCR fragment was digested with *Xho*I and *Bgl*II and ligated into the pUC plasmid backbone amplified by PCR using pCAG-EGFP as a template, to generate pUC-rat Syp genomic DNA. Then PCR was performed using primers (5′-AAATGCTAAGCGGCCGCTAATCTGGTGAGT-GACAGATG-3′ and 5′-AATTACCGGTGGATCCGGAGAAGGAG-GTGGGCGCACC-3′) and pUC-rat Syp genomic DNA as a template. The PCR fragment was ligated with linker-EGFP excised from pCAG-PSD-95-EGFP with *Bam*HI and *Not*I using the In-Fusion HD Cloning Kit to generate Syp targeting vector (EGFP). Syp targeting vector (mCherry) was constructed by digesting Syp targeting vector (EGFP) with *Bam*HI and *Not*I, and replacing the coding region of EGFP with that of mCherry excised from pCAG-Syp-mCherry with *Bam*HI/*Not*I.

The restriction enzyme sites are underlined. Nucleotide sequences of the knock-in vectors used in this study are shown in Supplemental Table S2.

Genotyping

For genotyping of transfected neurons, genomic DNAs were purified from the cultured neurons using QIAamp DNA Mini Kit (Qiagen), and genomic PCRs were performed using PrimeSTAR GXL DNA Polymerase (Takara Bio, Shiga, Japan). To detect the knock-in alleles, nested PCRs were performed. The first PCRs were carried out in a reaction volume of 25 µl: one cycle of 98°C

for 4 min, 20 cycles of 98°C for 10 s, 60°C for 15 s, and 68°C for 1 min. Using 0.5 µl of the first PCR products as templates, the second PCRs were carried out in a reaction volume of 25 µl: one cycle of 98°C for 3 min, 25 cycles of 98°C for 10 s, 60°C for 10 s, and 68°C for 40 s.

For genotyping of neurons transfected with PSD-95 targeting vector (EGFP), the first PCR was performed with primers (5′-TCCTCTCCATTGGTCACTCTCTCCACT-3′ and 5′-GTGCAGATGAACTTCAGGGTCAGCTTG-3′) and the second PCR was performed with primers (5′-CATCTGTCACTTCCCCTTTGGCCAACC-3′ and 5′-GACACGCTGAACTTGTGGCCGTTTACG-3′, product size 1320 base pairs). For genotyping of neurons transfected with PSD-95 targeting vector (mCherry), the first PCR was performed with primers (5′-TCCTCTCCATTGGTCACTCTCTCCACT-3′ and 5′-TCGATCTCGAACTCGTGGCCGTTCACG-3′) and the second PCR was performed with primers (5′-ATATTCTCTGTCTCTTCCTGGCACC-3′ and 5′-GACACGCTGAACTTGTGGCCGTTTACG-3′, product size 1285 base pairs).

For genotyping of neurons transfected with Syp targeting vector (EGFP), the first PCR was performed with primers (5′-AGGACAGGTCAGCCAGGACCTGGAACG-3′ and 5′-GTGCAGATGAACTTCAGGGTCAGCTTG-3′) and the second PCR was performed with primers (5′-ATCTGTTATACATATGCATCTATGTGC-3′ and 5′-GACACGCTGAACTTGTGGCCGTTTACG-3′, product size 1320 base pairs).

For genotyping of neurons transfected with Syp targeting vector (mCherry), the first PCR was performed with primers (5′-AGGACAGGTCAGCCAGGACCTGGAACG-3′ and 5′-TCGATCTCGAACTCGTGGCCGTTCACG-3′) and the second PCR was performed with primers (5′-ATCTGTTATACATATGCATCTATGTGC-3′ and 5′-GAAGCGCATGAACTCCTTGATGATGGC-3′, product size 1332 base pairs).

Electroporated PSD-95 targeting vector (EGFP), PSD-95 targeting vector (mCherry), Syp targeting vector (EGFP), and Syp targeting vector (mCherry) were detected with primer sets (5′-GGGAAGCACTGCATCCTCGATGTC-3′ and 5′-GACACGCTGAACTTGTGGCCGTTTACG-3′, product size 1191 base pairs, 5′-GGGAAGCACTGCATCCTCGATGTC-3′ and 5′ GAAGCGCATGAACTCCTTGATGATGGC-3′, product size 1156 base pairs, 5′-TTGAGACAGGGTCTACTTATATAGC-3′ and 5′-GACACGCTGAACTTGTGGCCGTTTACG-3′, product size 1122 base pairs, 5′-TTGAGACAGGGTCTACTTATATAGC-3′ and 5′-GAAGCGCATGAACTCCTTGATGATGGC-3′, product size 1087 base pairs, respectively) and the following conditions: one cycle of 98°C for 4 min, 35 cycles of 98°C for 10 s, 65°C for 10 s, and 68°C for 30 s. *Actb* was detected by genomic PCR using primers (5′-ATGTACGTAGCCATCCAGGCTGT-3′ and 5′-AGCTGTGGTGGTGAAGCTGTAG-3′, product size 219 base pairs) and the following conditions: one cycle of 98°C for 4 min, 35 cycles of 98°C for 10 s, 60°C for 15 s, and 68°C for 30 s.

To detect the *PSD-95* and *Syp* knock-out alleles, genomic PCRs were performed with primers (5′-ATATCTCGAGTGATTGTCAACACGGACACCCTAG-3′ and 5′-ATGCGGTACCAGCTGTCACTCAGGTAGGCATTGC-3′; 5′-ATATCTCGAGCTGCACCAAGTGTACTTTGATGC-3′ and 5′-ATGCGGTACCTGAGGTGTTGAGTC CTGAAGTCAC-3′, respectively) and the following conditions: one cycle of 98°C for 4 min, 35 cycles of 98°C for 10 s, 60°C for 15 s, and 68°C for 30 s. The PCR products digested with *Xho*I and *Acc*65I were cloned into pBluescript II KS(–) (Agilent), and DNA sequences were determined by Sanger sequencing (Greiner Bio-One).

The restriction enzyme sites are underlined.

Antibodies and reagents

We used the following antibodies: a mouse monoclonal anti-GFP antibody (B-2) (Santa Cruz Biotechnology); a mouse monoclonal anti-PSD-95 antibody (6G6-1C9), rabbit monoclonal antibodies against Syp (YE269) and PSD-95 (EP2652Y) (Abcam); a mouse monoclonal anti-Syp antibody (#61012) (PROGEN); a rabbit polyclonal anti-RFP antibody (PM005) (MBL); a rabbit polyclonal anti-GFP antibody, a rat monoclonal anti-mCherry antibody (Thermo Fisher Scientific); mouse monoclonal antibodies against Map2 (2a+2b) (AP-20), β-actin (AC-15), and α-tubulin (B-5-1-2) (Sigma-Aldrich); HRP–conjugated secondary antibodies (DakoCytomation); and Alexa Fluor–conjugated secondary antibodies (Thermo Fisher Scientific). Filamentous-actin (F-actin) staining was performed with Alexa647–conjugated phalloidin (Thermo Fisher Scientific). Poly-L-lysine (PLL) was purchased from Sigma-Aldrich, and recombinant human BDNF (248-BD-025) was purchased from R&D Systems.

Primary neuronal culture, transfection, and stimulation

Primary cortical and hippocampal neurons were prepared from E18 Wistar/ST rat brains as described previously (Oinuma *et al.*, 2004; Iwasawa *et al.*, 2012; Matsuda *et al.*, 2019). The dissociated neurons were seeded on PLL-coated glass coverslips (circular, 13 mm in diameter; Matsunami Glass, Osaka, Japan) at a density of 3×10^4 cells, or PLL-coated plastic cell culture dishes (35 mm in diameter at a density of 2×10^5, 60 mm in diameter at a density of 5×10^5 cells, or 100 mm in diameter at a density of 1×10^6 cells) in low glucose DMEM (Nissui Pharmaceutical, Tokyo, Japan) containing 10% fetal bovine serum (FBS), 4 mM glutamine, 100 U/ml penicillin, and 0.1 mg/ml streptomycin and cultured under humidified air containing 5% CO_2 at 37°C. After 4 h, the medium was replaced with Neurobasal medium (Thermo Fisher Scientific) containing 2% B27 supplement (Thermo Fisher Scientific), 0.5 mM GlutaMAX (Thermo Fisher Scientific), 50 U/ml penicillin (FUJIFILM Wako Pure Chemical, Osaka, Japan), and 0.05 mg/ml streptomycin (FUJIFILM Wako Pure Chemical, Osaka, Japan), and neurons were cultured under humidified air containing 5% CO_2 at 37°C. For lipofection experiments, neurons were transfected with the indicated plasmids at 1 DIV with Lipofectamine 2000 (Thermo Fisher Scientific) according to the manufacturer's instructions.

For nucleofection experiments, transfection was performed as described previously (Tasaka *et al.*, 2012; Umeda *et al.*, 2015; Matsuda *et al.*, 2019) using the Rat Neuron Nucleofector Kit (Lonza) following the manufacturer's instructions using the program (o-003) of the Nucleofector Device (Lonza). The transfection efficiency (GFP-positive cells/DAPI [4′,6-diamidino-2-phenylindole]-positive cells) determined at 1.5 DIV using pCAG-EGFP was 94.7 ± 0.918%, and 100% of GFP-positive cells were positive for a neuronal marker, Tuj1, confirming that contamination of nonneuronal cells including glial cells in the primary rat cortical neurons is negligible (Matsuda *et al.*, 2019).

BDNF was reconstituted at 50 µg/ml in phosphate-buffered saline (PBS), and BDNF treatment (50 ng/ml) was performed for 1 h. To depolarize neurons, cells were treated for 15 min with 20 mM KCl (Nacalai Tesque, Kyoto, Japan) using NaCl (Nacalai Tesque, Kyoto, Japan) as the corresponding vehicle control.

RT-PCR

Total RNAs were extracted from primary cultured neurons using the RNeasy Mini Kit (Qiagen), and reverse-transcribed using SuperScript III Reverse Transcriptase (Thermo Fisher Scientific) according to the manufacturer's instructions. To detect the expression of *PSD-95-EGFP* fusion gene, RT-PCR was carried out using KOD FX Neo DNA polymerase (Toyobo, Osaka, Japan), and primer sets

(5′-TGCACTATGCTCGTCCCATCATCATC-3′ and 5′-GACACGCTGAACTTGTGGCCGTTTACG -3′, product size 754 base pairs) under the following conditions: one cycle of 98 °C for 3 min, 38 cycles of 98 °C for 10 s, and 68 °C for 1 min. The expression of *mCherry* from pCAG-mCherry was detected by RT-PCR with primers (5′-TAACATGGCCATCATCAAGGAGTTC-3′ and 5′-AGCCCATGGTCTTCTTCTGCATTAC-3′, product size 309 base pairs) under the following conditions: one cycle of 98°C for 3 min, 35 cycles of 98°C for 10 s, 62°C for 15 s, and 68°C for 30 s. The expression of *Actb* was detected by RT-PCR with primers (5′-ATGTACGTAGCCATCCAGGCTGT-3′ and 5′-AGCTGTGGTGGTGAAGCTGTAG-3′, product size 419 base pairs) under the following conditions: one cycle of 98°C for 3 min, 25 cycles of 98°C for 10 s, 60°C for 10 s, and 68°C for 30 s. Quantitative RT-PCR was performed on a CFX96 Touch Real-Time PCR Detection System (Bio-Rad) using KOD SYBR qPCR Mix (Toyobo, Osaka, Japan) and the primers described above. All qRT-PCR samples were analyzed in triplicate. The expression level of *PSD-95-EGFP* fusion gene for each sample was normalized to the expression of *mCherry* from pCAG-mCherry as the transfection control.

Immunoblotting

Proteins were separated by SDS–PAGE and were electrophoretically transferred onto a polyvinylidene difluoride membrane (Millipore). The membrane was blocked with 3% low-fat milk (Nacalai Tesque, Kyoto, Japan) in Tris-buffered saline (TBS) and then incubated with primary antibodies in TBS containing 3% low-fat milk or Can Get Signal immunoreaction enhancer solution (Toyobo, Osaka, Japan) for 16 h at 4°C. The primary antibodies were detected with HRP–conjugated secondary antibodies and a Chemiluminescence Detection Kit (Chemi-Lumi One; Nacalai Tesque, Kyoto, Japan). Images were captured using an ImageQuant LAS4000 mini analyzer (GE Healthcare) equipped with ImageQuant TL software (GE Healthcare) for densitometric analysis.

Immunofluorescence microscopy

Primary cultured neurons on coverslips were fixed with 4% paraformaldehyde (PFA) in PBS for 20 min. After residual PFA had been quenched with 50 mM NH_4Cl in PBS for 10 min, cells were permeabilized with the buffer (0.5% Triton X-100, 50 mM NaCl, 300 mM sucrose, 10 mM PIPES, pH 6.8, and 3 mM $MgCl_2$) for 10 min and incubated with 10% FBS in PBS for 30 min. Cells were incubated with the first antibodies for 16 h at 4°C, followed by incubation with Alexa–conjugated secondary antibodies and Alexa–conjugated phalloidin for 1 h at room temperature. The cells on coverslips were mounted in 90% glycerol containing 0.1% *p*-phenylenediamine dihydrochloride in PBS or Prolong Gold antifade reagent (Thermo Fisher Scientific).

Epifluorescence images were photographed at room temperature with a DP80 digital camera system (Olympus) equipped with BX63 upright epifluorescence microscope system (Olympus) with 10× NA 0.40, 20× NA 0.75, and 40× NA 0.95 UPlanSApo objectives (Olympus) and cellSens Dimension software (Olympus).

To obtain a z-plane confocal image, optical sections of images were captured through the cell in 0.20-µm steps using a laser-scanning confocal imaging system (FLUOVIEW FV1000-D; Olympus) and a microscope equipped with a spectral system (IX81-S; Olympus) with a 60× NA 1.35 or 100× NA 1.40 oil objective (Olympus) at room temperature.

Superresolution images (up to 120 nm of maximum resolution according to the manufacturer's performance evaluation) were obtained at room temperature with FV-OSR superresolution system (Olympus) in conjugation with the FV1000-D system and the FV12-HSD high-sensitivity Gallium Arsenide Phosphide detectors (Olympus) using a 100× NA 1.49 UApoN TIRFM, oil objective.

For live-cell TIRF microscopy, we used a custom-built microscope comprised of an inverted microscope with Z-drift focus compensation module (IX83-ZDC; Olympus) equipped with an illumination system for TIRFM (IX2-RFAEVA-2; Olympus) and a 60× objective (UApoN TIRFM, oil, NA 1.49; Olympus). Neurons were cultured on PLL-coated glass bottom dishes (MatTek Corporation), and the cells were enclosed in a stage-top incubator (INU; Tokai Hit, Shizuoka, Japan) to maintain the cell culture conditions of 37°C, 5% CO_2/95% air, and high humidity. EGFP or mCherry adjacent to the cover glass–cell interface was excited with evanescent waves of a 488-nm solid-state 30 mW laser (Melles Griot) or a 561-nm solid-state 20 mW laser (Sapphire 561; Coherent), and its emission was collected through band-pass filter sets (ET-GFP and ET-mCherry; Chroma Technology) together with the DualView beam splitter for emission separation (DV2, Roper Scientific). Images were acquired with MetaMorph version 7.7 software (Molecular Devices) and a high-speed EMCCD digital camera (ImagEMX2; Hamamatsu Photonics, Shizuoka, Japan) with 500× EM-Gain setting. Images were acquired every 3 min starting from 1 h before until 1 h after the onset of BDNF application.

All images were processed with MetaMorph version 7.7 software (Molecular Devices) and ImageJ software (http://rsbweb.nih.gov/ij/) and arranged and labeled using Photoshop CS5.1 (Adobe) and Canvas Draw4 (ACD Systems).

Data analysis

Protein densitometry analysis was performed using ImageQuant TL software (GE Healthcare) and the immunoblot data shown are representative of three independent experiments.

Quantification of dendritic spine morphology was performed as described previously (El-Husseini *et al.*, 2000; Ishikawa *et al.*, 2003). Quantification of dendritic protrusion density was performed using cellSens Dimension software (Olympus). Protrusions were counted along 50 µm of dendrite segments. Dendritic spines were defined as <6 µm dendritic protrusions with mushroom-shaped heads or stubby-shaped structures as determined by CAG-mCherry fluorescence. At least 50 dendritic segments from 20 neurons per experimental group were collected from three independent experiments, and statistical differences for multiple groups were assessed by one-way analysis of variance (ANOVA) and post hoc test (Dunnett) or Student's *t* test using Prism version 5f software (GraphPad).

Statistics

Data are presented as the mean ± SEM. Statistical analyses were performed using Prism version 5f software (GraphPad Software). Differences at the level of $p < 0.05$ were considered statistically significant. Multiple comparisons were performed using one-way ANOVA, followed by post hoc test. Actual *p* values have been provided on the graphs in the figures.

ACKNOWLEDGMENTS

We thank Feng Zhang and Carlos Lois for plasmids, Takuro Tojima for advice on building the TIRFM imaging system, and Tadashi Uemura and Ryoichiro Kageyama for discussions regarding this project. This work was supported by the Japan Science and Technology Agency PRESTO Project (Development and Function of Neuronal Networks) to I.O. and T.M.; Grants-in-aid for Scientific Research from the Ministry of Education, Culture, Sports, Science and Technology of Japan (Scientific Research on Innovative Areas 17H05773 [I.O.] and Scientific Research [C] 17K07340 [I.O.]; and

grants from the Takeda Science Foundation (I.O.), the Hyogo Science and Technology Association (I.O.), the Kato Memorial Bioscience Foundation (I.O.), the Futaba Electronics Memorial Foundation (I.O.), and the Shimadzu Science Foundation (T.M.).

REFERENCES

Acosta S, Fiore L, Carota IA, Oliver G (2018). Use of two gRNAs for CRISPR/Cas9 improves bi-allelic homologous recombination efficiency in mouse embryonic stem cells. Genesis 56, e23212.

Bao J, Lin H, Ouyang Y, Lei D, Osman A, Kim TW, Mei L, Dai P, Ohlemiller KK, Ambron RT (2004). Activity-dependent transcription regulation of PSD-95 by neuregulin-1 and Eos. Nat Neurosci 7, 1250–1258.

Béïque JC, Andrade R (2003). PSD-95 regulates synaptic transmission and plasticity in rat cerebral cortex. J Physiol 546, 859–867.

Cameron PL, Südhof TC, Jahn R, De Camilli P (1991). Colocalization of synaptophysin with transferrin receptors: implications for synaptic vesicle biogenesis. J Cell Biol 115, 151–164.

Chen X, Vinade L, Leapman RD, Petersen JD, Nakagawa T, Phillips TM, Sheng M, Reese TS (2005). Mass of the postsynaptic density and enumeration of three key molecules. Proc Natl Acad Sci USA 102, 11551–11556.

Cheng A, Wan R, Yang JL, Kamimura N, Son TG, Ouyang X, Luo Y, Okun E, Mattson MP (2012). Involvement of PGC-1α in the formation and maintenance of neuronal dendritic spines. Nat Commun 3, 1250.

Chu VT, Weber T, Wefers B, Wurst W, Sander S, Rajewsky K, Kühn R (2015). Increasing the efficiency of homology-directed repair for CRISPR-Cas9-induced precise gene editing in mammalian cells. Nat Biotechnol 33, 543–548.

Colledge M, Snyder EM, Crozier RA, Soderling JA, Jin Y, Langeberg LK, Lu H, Bear MF, Scott JD (2003). Ubiquitination regulates PSD-95 degradation and AMPA receptor surface expression. Neuron 40, 595–607.

Cong L, Ran FA, Cox D, Lin S, Barretto R, Habib N, Hsu PD, Wu X, Jiang W, Marraffini LA, Zhang F (2013). Multiplex genome engineering using CRISPR/Cas systems. Science 339, 819–823.

Cox DB, Platt RJ, Zhang F (2015). Therapeutic genome editing: prospects and challenges. Nat Med 21, 121–131.

Distler JH, Jüngel A, Kurowska-Stolarska M, Michel BA, Gay RE, Gay S, Distler O (2005). Nucleofection: a new, highly efficient transfection method for primary human keratinocytes. Exp Dermatol 14, 315–320.

Doench JG, Hartenian E, Graham DB, Tothova Z, Hegde M, Smith I, Sullender M, Ebert BL, Xavier RJ, Root DE (2014). Rational design of highly active sgRNAs for CRISPR-Cas9-mediated gene inactivation. Nat Biotechnol 32, 1262–1267.

Doudna JA, Charpentier E (2014). Genome editing. The new frontier of genome engineering with CRISPR-Cas9. Science 346, 1258096.

Ehrlich I, Malinow R (2004). Postsynaptic density 95 controls AMPA receptor incorporation during long-term potentiation and experience-driven synaptic plasticity. J Neurosci 24, 916–927.

El-Husseini AE, Schnell E, Chetkovich DM, Nicoll RA, Bredt DS (2000). PSD-95 involvement in maturation of excitatory synapses. Science 290, 1364–1368.

Fortin DA, Tillo SE, Yang G, Rah JC, Melander JB, Bai S, Soler-Cedeño O, Qin M, Zemelman BV, Guo C, *et al.* (2014). Live imaging of endogenous PSD-95 using ENABLED: a conditional strategy to fluorescently label endogenous proteins. J Neurosci 34, 16698–16712.

Gaj T, Gersbach CA, Barbas CF 3rd (2013). ZFN, TALEN, CRISPR/Cas-based methods for genome engineering. Trends Biotechnol 31, 397–405.

Gross GG, Junge JA, Mora RJ, Kwon HB, Olson CA, Takahashi TT, Liman ER, Ellis-Davies GC, McGee AW, Sabatini BL, *et al.* (2013). Recombinant probes for visualizing endogenous synaptic proteins in living neurons. Neuron 78, 971–985.

Heidenreich M, Zhang F (2016). Applications of CRISPR-Cas systems in neuroscience. Nat Rev Neurosci 17, 36–44.

Hering H, Sheng M (2001). Dendritic spines: structure, dynamics and regulation. Nat Rev Neurosci 12, 880–888.

Heyer WD, Ehmsen KT, Liu J (2010). Regulation of homologous recombination in eukaryotes. Annu Rev Genet 44, 113–139.

Hsu PD, Lander ES, Zhang F (2014). Development and applications of CRISPR-Cas9 for genome engineering. Cell 157, 1262–1278.

Incontro S, Asensio CS, Edwards RH, Nicoll RA (2014). Efficient, complete deletion of synaptic proteins using CRISPR. Neuron 83, 1051–1057.

Ishikawa Y, Katoh H, Negishi M (2003). A role of Rnd1 GTPase in dendritic spine formation in hippocampal neurons. J Neurosci 23, 11065–11072.

Iwasawa N, Negishi M, Oinuma I (2012). R-Ras controls axon branching through afadin in cortical neurons. Mol Biol Cell 23, 2793–2804.

Iyama T, Wilson 3rd DM (2013). DNA repair mechanisms in dividing and non-dividing cells. DNA Repair 12, 620–636.

Jang DE, Lee LY, Lee JH, Koo OJ, Bae HS, Jung MH, Bae JH, Hwang WS, Chang YJ, Lee YH, *et al.* (2018). Multiple sgRNAs with overlapping sequences enhance CRISPR/Cas9-mediated knock-in efficiency. Exp Mol Med 50, 16.

Ji Y, Pang PT, Feng L, Lu B (2005). Cyclic AMP controls BDNF-induced TrkB phosphorylation and dendritic spine formation in mature hippocampal neurons. Nat Neurosci 8, 164–172.

Jinek M, Chylinski K, Fonfara I, Hauer M, Doudna JA, Charpentier E (2012). A programmable dual-RNA-guided DNA endonuclease in adaptive bacterial immunity. Science 337, 816–821.

Jourdi H, Iwakura Y, Narisawa-Saito M, Ibaraki K, Xiong H, Watanabe M, Hayashi Y, Takei N, Nawa H (2003). Brain-derived neurotrophic factor signal enhances and maintains the expression of AMPA receptor-associated PDZ proteins in developing cortical neurons. Dev Biol 263, 216–230.

Karra D, Dahm R (2010). Transfection techniques for neuronal cells. J Neurosci 30, 6171–6177.

Leal G, Comprido D, Duarte CB (2014). BDNF-induced local protein synthesis and synaptic plasticity. Neuropharmacology 76, 639–656.

Mali P, Yang L, Esvelt KM, Aach J, Guell M, DiCarlo JE, Norville JE, Church GM (2013). RNA-guided human genome engineering via Cas9. Science 339, 823–826.

Maruyama T, Dougan SK, Truttmann MC, Bilate AM, Ingram JR, Ploegh HL (2015). Increasing the efficiency of precise genome editing with CRISPR-Cas9 by inhibition of nonhomologous end joining. Nat Biotechnol 33, 538–542.

Matsuda T, Cepko CL (2004). Electroporation and RNA interference in the rodent retina in vivo and in vitro. Proc Natl Acad Sci USA 101, 16–22.

Matsuda T, Namura A, Oinuma I (2019). Dynamic spatiotemporal patterns of alternative splicing of an F-actin scaffold protein, afadin, during murine development. Gene 689, 56–68.

Mikuni T, Nishiyama J, Sun Y, Kamasawa N, Yasuda R (2016). High-throughput, high-resolution mapping of protein localization in mammalian brain by in vivo genome editing. Cell 165, 1803–1817.

Niwa H, Yamamura K, Miyazaki J (1991). Efficient selection for high-expression transfectants with a novel eukaryotic vector. Gene 108, 193–199.

Ohki EC, Tilkins ML, Ciccarone VC, Price PJ (2001). Improving the transfection efficiency of post-mitotic neurons. J Neurosci Methods 112, 95–99.

Oinuma I, Ishikawa Y, Katoh H, Negishi M (2004). The Semaphorin 4D receptor Plexin-B1 is a GTPase activating protein for R-Ras. Science 305, 862–865.

Platt RJ, Chen S, Zhou Y, Yim MJ, Swiech L, Kempton HR, Dahlman JE, Parnas O, Eisenhaure TM, Jovanovic M, *et al.* (2014). CRISPR-Cas9 knockin mice for genome editing and cancer modeling. Cell 159, 440–455.

Poo MM (2001). Neurotrophins as synaptic modulators. Nat Rev Neurosci 2, 24–32.

Saleh-Gohari N, Helleday T (2004). Conservative homologous recombination preferentially repairs DNA double-strand breaks in the S phase of the cell cycle in human cells. Nucleic Acids Res 32, 3683–3688.

Sander JD, Joung JK (2014). CRISPR-Cas systems for editing, regulating and targeting genomes. Nat Biotechnol 32, 347–355.

Shinmyo Y, Tanaka S, Tsunoda S, Hosomichi K, Tajima A, Kawasaki H (2016). CRISPR/Cas9-mediated gene knockout in the mouse brain using in utero electroporation. Sci Rep 6, 20611.

Stein V, House DR, Bredt DS, Nicoll RA (2003). Postsynaptic density-95 mimics and occludes hippocampal long-term potentiation and enhances long-term depression. J Neurosci 23, 5503–5506.

Straub C, Granger AJ, Saulnier JL, Sabatini BL (2014). CRISPR/Cas9-mediated gene knock-down in post-mitotic neurons. PLoS One 9, e105584.

Sugiyama Y, Kawabata I, Sobue K, Okabe S (2005). Determination of absolute protein numbers in single synapses by a GFP-based calibration technique. Nat Methods 2, 677–684.

Swiech L, Heidenreich M, Banerjee A, Habib N, Li Y, Trombetta J, Sur M, Zhang F (2015). In vivo interrogation of gene function in the mammalian brain using CRISPR-Cas9. Nat Biotechnol 33, 102–106.

Tasaka G, Negishi M, Oinuma I (2012). Semaphorin 4D/Plexin-B1-mediated M-Ras GAP activity regulates actin-based dendrite remodeling through Lamellipodin. J Neurosci 32, 8293–8305.

The ENCODE Project Consortium (2012). An integrated encyclopedia of DNA elements in the human genome. Nature 489, 57–74.

Tsunekawa Y, Terhune RK, Fujita I, Shitamukai A, Suetsugu T, Matsuzaki F (2016). Developing a de novo targeted knock-in method based on in utero electroporation into the mammalian brain. Development 143, 3216–3222.
Tyler WJ, Pozzo-Miller LD (2001). BDNF enhances quantal neurotransmitter release and increases the number of docked vesicles at the active zones of hippocampal excitatory synapses. J Neurosci 21, 4249–4258.
Uemura T, Mori T, Kurihara T, Kawase S, Koike R, Satoga M, Cao X, Li X, Yanagawa T, Sakurai T, *et al*. (2016). Fluorescent protein tagging of endogenous protein in brain neurons using CRISPR/Cas9-mediated knock-in and in utero electroporation techniques. Sci Rep 6, 35861.
Umeda K, Iwasawa N, Negishi M, Oinuma I (2015). A short splicing isoform of afadin suppresses the cortical axon branching in a dominant-negative manner. Mol Biol Cell 26, 1957–1970.
Vasquez KM, Marburger K, Intody Z, Wilson JH (2001). Manipulating the mammalian genome by homologous recombination. Proc Natl Acad Sci USA 98, 8403–8410.
Wang S, Sengel C, Emerson MM, Cepko CL (2014). A gene regulatory network controls the binary fate decision of rod and bipolar cells in the vertebrate retina. Dev Cell 30, 513–527.
Xue W, Chen S, Yin H, Tammela T, Papagiannakopoulos T, Joshi NS, Cai W, Yang G, Bronson R, Crowley DG, *et al*. (2014). CRISPR-mediated direct mutation of cancer genes in the mouse liver. Nature 514, 380–384.
Yang H, Wang H, Shivalila CS, Cheng AW, Shi L, Jaenisch R (2013). One-step generation of mice carrying reporter and conditional alleles by CRISPR/Cas-mediated genome engineering. Cell 154, 1370–1379.
Yin H, Xue W, Chen S, Bogorad RL, Benedetti E, Grompe M, Koteliansky V, Sharp PA, Jacks T, Anderson DG (2014). Genome editing with Cas9 in adult mice corrects a disease mutation and phenotype. Nat Biotechnol 32, 551–553.
Zhou J, Wang J, Shen B, Chen L, Su Y, Yang J, Zhang W, Tian X, Huang X (2014). Dual sgRNAs facilitate CRISPR/Cas9-mediated mouse genome targeting. FEBS J 281, 1717–1725.